MEASURING THE TOPOGRAPHY AND MOTION OF ROCK GLACIERS IN THE CORDILLERA PRINCIPAL, ARGENTINA

by

Adrienne Shumlich

A thesis submitted to the Faculty of the University of Delaware in partial fulfillment of the requirements for the degree of Master of Science in Geography

Summer 2018

© 2018 Adrienne Shumlich
All Rights Reserved

MEASURING THE TOPOGRAPHY AND MOTION OF ROCK GLACIERS IN THE CORDILLERA PRINCIPAL, ARGENTINA

by

Adrienne Shumlich

Approved: _____
Michael A. O'Neal, Ph.D.
Professor in charge of thesis on behalf of the Advisory Committee

Approved: _____
Delphis Levia, Ph.D.
Chair of the Department of Geography

Approved: _____
Estella Atekwana, Ph.D.
Dean of Earth Ocean and Environment

Approved: _____
Douglas J. Doren, Ph.D.
Interim Vice Provost for Graduate and Professional Education

ACKNOWLEDGMENTS

First and foremost, I would like to thank Dr. Andres Meglioli, without whom this thesis would not have been possible. I would like to thank him for the incredible opportunity to visit these field sites on two occasions, the mentorship that he provided in the field, as well providing access to additional data. I am also extremely grateful for the mentorship I have received at the University of Delaware. Specifically, I would like to thank my advisor, Dr. Michael O'Neal for organizing my visits to the field, as well as his guidance in my research and writing. Without him believing in me and supporting me, the opportunity to take part in this exciting research opportunity exactly aligned with my interests would not have been possible. I am grateful for my committee members, Dr. Brian Hanson and Dr. Tracy DeLiberty for their guidance in this thesis as well as support outside of research. I would also like to thank Dr. Dana Veron who made extra effort to check in on me. Additionally, I am indebted to Dr. Cathleen Geiger, Dr. Del Levia, and the Geography department at the University of Delaware without whom my dreams of pursuing my Masters would not have been possible, and for making Newark feel like home.

Additionally, this thesis was possible by an accumulation of support that I have received from family, friends, and mentors throughout my life. I would like to thank my friends and family for their unwavering support. Specifically, I would like to thank my parents, sisters, and brother for always believing in me and providing me a solid foundation. I would also like to thank my friends Alexis Cunningham, Elahe Gange, and Julia Mickan, who were my rocks throughout the last two years in Newark. I

would also like to thank Dustin Duczek, who was the first person I told when I got accepted to University of Delaware and encouraged me from the start. I would also like to thank him for teaching me the importance of mental health above all else.

TABLE OF CONTENTS

LIST OF TABLES vii
LIST OF FIGURES viii
ABSTRACT xi

Chapter

1 INTRODUCTION 1

2 STUDY AREA 4

2.1 Location 4
2.2 Geology and Climate 4

3 METHODS 6

3.1 Close Range Digital Photogrammetry 6
3.2 RTK GPS 6

3.2.1 El Altar GPS Survey Points 7
3.2.2 QDM GPS Survey Points 8
3.2.3 Los Azules GPS Survey Points 8

3.3 Digital photogrammetry derivatives 8
3.4 ASTER and Derivatives 9
3.5 Physics of Expected Movement 9
3.6 Other Motion-Based Studies 11

4 RESULTS 12

4.1 Close Range Digital Photogrammetry and Derivatives 12

4.1.1 El Altar Topography 12
4.1.2 QDM Topography 13
4.1.3 Los Azules Topography 13

4.2 Motion from repeated GPS surveys 14

4.2.1 El Altar Motion 14
4.2.2 QDM 16
4.2.3 Los Azules 17

4.3 ASTER Slope 18

5 DISCUSSION 20

6 CONCLUSION 25

FIGURES 26
TABLES 46
REFERENCES 51

Appendix

A MOTION 53

LIST OF TABLES

Table 1 Station numbers and the dates that RTK GPS data were collected for all locations at the El Altar and QDM study areas. 46

Table 2 Station numbers and the dates that RTK GPS data were collected for all locations at the Los Azules study area. 47

Table 3 El Altar and QDM station numbers and their associated bearing, distance, and elevation change for all recorded dates. 48

Table 4 Los Azules station numbers and their associated bearing, distance, and elevation change for all recorded dates. 49

Table 5 Rock glacier movement in locations around the world along with associated region, location, and elevation. Movement data given in m yr^{-1}. 50

LIST OF FIGURES

Figure 1 Locations of El Altar and Los Azules study site which are located in the High Andes in Argentina in close proximity to the Chilean border Specifically, El Altar and QDM are located at 31° 28′ S 70° 31′ W, and Los Azules is at 31° 05′ S 70° 14′ W. 26

Figure 2 El Altar rock glacier obtained from Digital Globe on 3/30/2010 from Google Earth Pro with locations of 11 motion-monitoring stakes and 4 off-glacier control stakes (MO15, MO14, MO13, and MO12) marked by labelled dots. In the cluster of 4 stakes (MO01 through MO04), only MO03 is used for statistical purposes because it was measured over the longest period: 83 months. The other 3 stakes in that cluster are displayed in Appendix A but are not included in statistical analysis. 27

Figure 3 QDM rock glacier obtained from Digital Globe on 3/30/2010 from Google Earth Pro with locations of three motion-monitoring stakes marked by labelled dots. The stakes were placed upglacier, midglacier, and near-terminus along an estimated central flowline based on the surface topography. 28

Figure 4 Los Azules rock glacier obtained from Digital Globe on 2/15/2004 from Google Earth Pro with locations of 10 motion-monitoring stakes marked by labelled dots. Motion from stakes MAW3, MAW2, MAW1, MAE3, and MAW5 captured by the orthoimagery, and the additional 5 stakes examined using ASTER imagery. The road, visible as a light curve in the upper part of the image, constructed just above the estimated position of the glacier. 29

Figure 5 Digital elevation model (DEM) of El Altar rock glacier rendered from stitching areal images captured in March, 2017 using close-range digital photogrammetry survey methods. Stake locations labeled and depicted with points and the image displayed with 5 m contour intervals. The glacier has a general trend of decreasing elevation down glacier towards its tongue. 30

Figure 6 A 5m x 5m slope raster of El Altar rock glacier displays an average slope of approximately 32° on the upper transverse lobes. The flatter lower portion has a slope of approximately 15°. 31

Figure 7 Digital elevation model (DEM) of QDM rock glacier rendered from stitching areal images captured in March 2017 using close-range digital photogrammetry survey methods. Stake locations labeled and depicted with points and the image displayed with 5 m contour intervals. The glacier has a general trend of decreasing elevation down glacier towards its tongue. 32

Figure 8 A 5m x 5m slope raster of QDM rock glacier. QDMRG-7L is located on a slope of 14°, QDMRG-6L is located on a slope of 22°, and QDMRG-5L is located on a slope of 18°. 33

Figure 9 Digital elevation model (DEM) of Los Azules rock glacier rendered from stitching areal images captured in March 2017 using close-range digital photogrammetry survey methods. Stake locations labeled and depicted with points and the image displayed with 5 m contour intervals. The glacier has a general trend of decreasing elevation down glacier towards its tongue. 34

Figure 10 A 5m x 5m slope of Los Azules rock glacier. MAW3 is located on the most gradual slope (8°), and MAE3 is located on the steepest slope (31°). The remaining stakes are located on a slope ranging from 16° to 21°. 35

Figure 11 El Altar rock glacier motion vectors and associated speeds in m yr^{-1}. Image obtained from Digital Globe on 3/30/2010 from Google Earth Pro. Control points which recorded negligible movement are labeled with triangles. 36

Figure 12 Comparison of rate of motion reported in m yr^{-1} with elevation reported in masl obtained from the DEM created by stitching aerial imagery. A) El Altar rock glacier; B) QDM rock glacier; C) Los Azules rock glacier. 37

Figure 13 QDM rock glacier motion vectors and associated speeds in m yr^{-1}. Image obtained from Digital Globe on 3/30/2010 from Google Earth Pro and motion data gathered from RTK GPS. QMRG-6L is centermost stake and the fastest moving, and QMRG-7L is the uppermost and slowest moving of the stakes examined. 38

Figure 14 Comparison of rate of motion reported in m yr^{-1} with slope reported in degrees obtained from the slope models created by stitching aerial imagery. A) El Altar rock glacier; B) QDM rock glacier; C) Los Azules rock glacier. 39

Figure 15 Los Azules rock glacier motion vectors and associated speeds in m yr^{-1}. Image obtained from Digital Globe on 2/15/2004 from Google Earth Pro. All stakes observed move at a significantly slower rate than El Altar and QDM rock glaciers. The fastest moving stake MAE2, which is located on the uppermost portion of the rock glacier flowing to the eastern accumulation zone. The slowest moving stake is MAW3, located on the peak of a transverse ridge flowing to the western accumulation zone. 40

Figure 16 A slope model of the El Altar rock glacier created by using ASTER imagery. All stakes on glacier fall within a slope range of 0°-20°. MO19 is located on the steepest slope (13°), and MO07 is located on the most gradual slope (7°). 41

Figure 17 A slope model of the QDM rock glacier created by using ASTER imagery. QMRG-6L is located on the steepest slope (22°) and QMRG-7L is located on the most gradual slope (19°). 42

Figure 18 A slope model of the Los Azules rock glacier created by using ASTER imagery. The upper and tongue portion of the rock glacier contain the most gradual slopes (~5°-10°), whereas the center portion contains the steepest slopes (20°-35°). 43

Figure 19 Comparison of rate of motion reported in m yr^{-1} with slope reported in degrees obtained from the slope models created by obtaining ASTER imagery. A) El Altar rock glacier; B) QDM rock glacier; C) Los Azules rock glacier. 44

Figure 20 Comparison of rate of motion reported in m yr^{-1} with $(h\alpha)^2$ where h is the thickness of the rock glacier obtained from subtracting stake elevations with adjacent valley elevations, and α is the slope of the stake obtained from the slope models created from stitching aerial imagery. A) El Altar rock glacier; B) QDM rock glacier; C) Los Azules rock glacier. 45

ABSTRACT

GPS and digital photogrammetry were used to obtain topographic and motion data for the El Altar, QDM, and Los Azules Rock Glaciers in the High Dry Andes of Argentina. A total of 21 survey stations (8 at El Altar, 3 at QDM, and 10 at Los Azules) were monitored between AD 2010 and 2017 at various intervals as allowed by funding and weather conditions at the study locales. Rates of motion were compared with elevation, local slope, and rock glacier thickness at each station. Results suggest that all three landforms or portions of the glaciers are active rock glaciers, but no single correlation explains the nature of movement for all the study landforms. El Altar's motion is correlated with elevation and not slope and suggests an upper portion moving approximately 2 to 5 times faster than motion along the terminal margin (ca. 0.16 m yr^{-1} vs. 0.2 m yr^{-1}). Those rates, coupled with the lack of ice or melt water at the margin suggests much of this landforms motion likely occurs as creep much slower than velocities of typical ice rich glacial forms. This indicates the upper portion is likely active, whereas the lower portion is likely inactive. The QDM rock glacier, where ice has been identified within a few meters of the terminus, shows a significant correlation ($R^2 = 0.97$, Figure 18b) between local slope and rate of motion. Los Azules, despite having a known ice rich margin, shows little down-valley movement at rates of 0.04 m yr^{-1}. This slow movement is difficult to explain but may be a result of the multiple accumulation areas that are generally transverse to the valley in which they accumulate. This results in a landform that is poorly organized topographically, with hummocky topography and slow rate of motion. These results emphasize that these landforms have a complex response to both internal ice and surface topography. Our results, most of which would be impossible without high resolution topographic

data, underscore the value of coupling aerial imagery with sparse data like the GPS measurements to provide insight for future analyses focused on ice presence and volume.

Chapter 1

INTRODUCTION

To mitigate the loss of ice as a potential water resource, the Argentine government became the first country in the world to instate a National Glacier Act, which limits anthropogenic alteration of glaciers, including both surface and buried ice forms. With this law, adopted on 30 September 2010, the government recognized icy landscapes as important water reservoirs for human consumption, agriculture, and watershed recharge. The extent to which ice-rich landforms are significant contributors to the water budget in the High Dry Andes, which extends from the Atacama Desert at 20°S to approximately 45°S in Argentina, is presently unknown. This uncertainty largely arises from the thick debris cover in much of the region that makes it difficult to distinguish between landforms with buried ice and relict landforms that once contained ice. While the National Glacier Act is potentially helpful for preserving water resources, misidentification of ice-free landforms as those with may hinder or prevent productive development of resources in the region, especially the mining of metal deposits. Thus, there is a strong impetus to accurately classify this terrain.

In many midlatitude regions, identifying icy landforms is a relatively straightforward task because exposed surface ice tends to be visibly obvious. However, the High Dry Andes is a low-precipitation, largely vegetation-free area with an abundance of sediment that often produces landforms such as rock glaciers, which may have substantial interstitial and subsurface ice but no or limited visible surface

ice. Rock glaciers typically form on high mountains or in dry polar terrain and are generally regarded as the main demonstration of mountain permafrost (Barsch, 1996; Berthling, 2011). Rock glaciers are composed of rock debris eroded from surrounding headwalls, with interstitial ice forming within the pores of the debris from compacted sedimentary ice, freezing rain, freezing meltwater, or freezing groundwater (Clark et al., 1998). Rock glaciers generally display steep slopes on their margins and termini, and tongue- or lobate-shaped, with ridges, furrows, and occasionally lobes on their surface. When they are active, they flow downslope over time, while those that are inactive (in which the majority of ice is depleted) do not flow but may retain their "glacier-like" geomorphic terrains. In the dry Andes, surface features indicating past presence of a rock glacier may persist long after the activity that formed them ceases because there are few mechanisms for eroding or denuding them over time (Capps 1910).

The research presented in this thesis continues a line of inquiry directed at mapping and explaining the presence of debris-covered glacial and periglacial landforms at two locales in the High Dry Andes. Schreiber (2015) presented a method of predicting buried ice based on environmental factors including ground temperature, elevation and direct insolation. To examine these methods, Trzinski (2017) identified and statistically analyzed existing glacial and periglacial landforms in the High Dry Andes in an attempt to classify forms using climatic and physiographic variables. The results from Trzinski's study indicated that the methods described in Schreiber (2015) well identified likely permafrost zones but were not a precise method of predicting the distribution of rock glaciers and similar landforms. Thus, though significant progress

has been made in terms of practical identification of active versus relict rock glaciers, the issue remains both challenging and complicated.

This study seeks to improve our understanding of rock glaciers in the High Dry Andes by evaluating the rates and spatial patterns of movement measured at three sites over an 8-year period. Specifically, to accomplish this goal, we 1) collected and analyzed spatial movement of different parts of each rock glacier using RTK GPS; 2) obtained detailed topographic data of each rock glacier from photogrammetric techniques applied to high-resolution aerial imagery and the ASTER Global Digital Elevation Model (GDEM); 3) compared the topography obtained from photogrammetric techniques and ASTER GDEM with the GPS data; 4) used simplified glacier dynamics to evaluate the rock glacier motion in terms of expected movement; and 5) compared these results with other motion-based studies, including those of the same study area and analogous landforms around the world. The results of this study have significant implications for responsible development in the region because they will influence decisions about allowance or disallowance of sites for potential resource extraction in accordance with the National Glacier Act.

Chapter 2

STUDY AREA

2.1 Location

The three locales used for this study, each with a single rock glacier, are known to those working in the Dry Andes as El Altar, QDM, and Los Azules. All are located within the Cordillera Principal of San Juan Province, Argentina, within the Dry Andes section of the Andes Mountain range (Figure 1). Peaks at the study sites range from 3700 m to 4200 m, while valley bottoms in the studied areas are above 3000 m.

2.2 Geology and Climate

The central Andes formed as a result of the continuous tectonic subduction of the Nazca Plate under the South American plate during the Cenozoic. The mountain range was subsequently subjected to glaciations at all scales, shaping the current mountain forms via erosion (Oncken, et al., 2006). Since the last glacial maximum, the region has had few ice-rich glaciers positioned on higher peaks. Many of the previously glacierized areas in high elevation terrain display signs of recent or active impacts of snow and ice (e.g., patterned ground, frost shattering, solifluction, rock glaciers, protalus ramparts).

The central Andes are located at the subtropical high-pressure region of atmospheric downwelling associated with the Hadley cell, diverging at the surface into tropical easterlies and southern midlatitude westerlies. At the latitude of the study sites, the extreme height of the Andes forces weather patterns coming from the Pacific to precipitate onto the western slopes. In contrast, the eastern side of the mountains is extremely arid, with conditions similar to desert regions at the same latitude in western

Africa and Australia (Houston and Hartley, 2003; Villagrán and Hinojosa, 1997). At the study sites, summers are generally dry and sunny with most precipitation falling during winter, though recent winters have been relatively dry.

Physical weathering dominates in high alpine and high latitude climates because temperatures are low and chemical weathering is typically slow. However, the small amount of precipitation that falls in this area significantly limits weathering rates. The primary process of weathering in this location is freeze-thaw weathering (especially frost shatter), in which precipitation fills pore space freezes and expands, causing the creation of fissures and eventually the breakdown of bedrock. In the study sites, the dominant freeze-thaw processes and subsequent movement of materials are readily visible owing to the lack of vegetation, presenting a unique opportunity to examine the landscape as a window into the past.

Chapter 3

METHODS

3.1 Close Range Digital Photogrammetry

Close-range aerial images, required for subsequent photogrammetric analyses in this study, were collected in March 2017 (El Altar and Los Azules) and March 2018 (QDM). A small, commercially available quadcopter with a 16 megapixel camera was used to collect RGB JPEG images in 5 second intervals as close to nadir as wind conditions allowed. The entirety of each landform was flown as close to midday as possible and in flights of less than 45 minutes to minimize the effects of shadows.

3.2 RTK GPS

Motion of the study rock glaciers (El Altar, QDM, and Los Azules) was measured at several survey stations on each glacier between AD 2010 and 2017 using real-time kinematic GPS (Trimble R6-RTK instantaneous positioning by correction transmission by ultra-high frequency). At each survey station, iron stakes were driven vertically into the surface debris and cemented in place. Most points were chosen to establish a longitudinal profile near the center of each glacier along an estimated flowline with several locations selected along the along the axis of longitudinal flow. These measurements had planimetric (x, y) accuracy of 1 mm to 5 mm and altimeter (z) accuracy of 3 mm to 6 mm. The measurements were gathered from two separate bases (the same bases were used for each survey station at a given rock glacier) and those measurements were averaged to obtain a single set of coordinates. The two bases were located in areas from which the entire survey area was visible. All coordinates are expressed in the POSGAR reference system (a geodetic coordinate system for Argentina). Each RTK survey also included survey stations on adjacent stable rock

surfaces to allow for differential motion calculations over time (2 additional survey stations at QDM, 4 at El Altar, and 2 at Los Azules). Frequency of data collection was dictated by weather (i.e., snowfall preventing site access), funding availability, site accessibility, as well as perceived need (i.e., removing stakes that are deemed close to other stakes, or adding stakes in locations that appeared to be changing rapidly or were overlooked in initial surveys). As such, dates of first and last measurement differ at both the site and station survey level (Tables 1 and 2).

Motions of the glacier points are sufficiently small that time variations of the velocities (differences between time-adjacent measurements) may indicate consistency of flow but probably should not be used to discuss short-term variations in rock-glacier speed. The spatial difference between the first and last measurements of each point provides a smoother, time-averaged estimate of the general velocity of each point, from which an annual average that characterizes AD 2010 to 2017 was calculated. To display the annual average and direction of movement, motion vectors were created using unique symbols for individual years (Appendix A).

3.2.1 El Altar GPS Survey Points

At El Altar, multiyear movement was monitored at 15 locations, four of which were off-glacier control points (Figure 2). Five of the points provide a profile along an estimated centerline of flow, with two of these placed to resolve an apparent transition from an upper glacier to a lower glacier with slightly different orientation and slope. Three points provide motions near the lateral margins of the lower glacier. Three stakes were only briefly measured, and these are all in the proximity of one of the other lateral margin survey stations. Results from these briefly measured survey stations are reported in the summary tables but not included in statistical analyses.

3.2.2 QDM GPS Survey Points

Multi-year movement was monitored at three distinct locations on the QDM rock glacier (Figure 3). All are located on an estimated centerline of glacier flow, with the lowest at the snout. A central point is on hummocky terrain approximately 90 m from the terminal margin. The highest point is approximately 220 m from the terminal margin and is at the base of a talus slope fed from two different sediment sources (evident from slightly different sediment colours).

3.2.3 Los Azules GPS Survey Points

Examination of the Los Azules rock glacier from aerial imagery indicates a hummocky terrain with many potentially palimpsest and active forms merging together. The western portion of this complex assemblage has had a coherent flow pattern recently enough to be visible on the landscape, and five survey stations were monitored in an apparent central flowline of this surface feature (Figure 4). East of this feature is a hummocky terrain with clear indications of surface motion but less so of a coherent glacier system. Two survey stations were monitored in the upper portion of this region, roughly 70 m from a road that is taken as the probable upper limit of the glacier (visible in Figure 4), and one more was positioned near the center of the eastern part of the complex. The last two survey stations are located at the snout of the easternmost portion of the glacier complex.

3.3 Digital photogrammetry derivatives

Digital photogrammetric techniques were used to develop digital elevation models (DEMs) and subsequent slope and aspect derivatives for each landform from the aerial imagery. A typical workflow was followed, which includes manually selecting images that were obtained at intended altitudes and on or close to nadir.

Several benchmarks, added as control points to each of the images, were selected from static locations easily identified in all images (i.e., survey markers, large rocks, well caps, etc.). Images were then aligned based on these benchmarks using greatest likelihood matching (e.g., Morgan et al., 2017). The aligned photos were evaluated statistically to produce a point cloud (Agisoft, 2015). ESRI ArcGIS was then used to generate DEMs at 0.25-m ground sample distance for further imagery analysis.

Using the DEMs, rock glacier motion at each survey station was compared to local slope, aspect, and relief. For the slope, an average was calculated within a 5 m by 5 m area of each survey station. This allows the analysis to focus on a slope more indicative of the rock glaciers' overall behavior within that 25 m^2 area, rather than a small area that may be affected by local relief. The relationship between elevation and aspect with each survey station were simply taken from the 0.25 m ground sample distance DEM and derivatives.

3.4 ASTER and Derivatives

To further analyze the effect of slope on rate of motion, the ASTER GDEM dataset (with 30 m by 30 m spatial resolution) was processed to obtain a slope model. This technique was intended to provide a coarser landscape model that limits the effects of individual large boulders, swales, and small ridging features, as these are unlikely to provide a general characterization of rock glacier motion.

3.5 Physics of Expected Movement

Because rock glacier motion is dependent on internal dynamics, a series of analyses was performed to evaluate if the motion of the study landforms correlates to basal shear stress, which takes into account thickness of the glacier, slope, and

acceleration due to gravity, and is the basis for determining rate of deformation (i.e., flow) of the glacier. For glaciers composed primarily of ice, a Glen (1955) power-law for flow would be integrated over the thickness of the glacier to estimate a total deformation velocity. However, rock glaciers in this area are known to be quite thin (10s of meters, rather than 100s) and, based on their dimensions, have very thin ice layers (< 10 m), so deformation velocities are not important. In the absence of large amounts of ice or water, the simple sliding law proposed by Weertman (1957), applying the Glen power law to flow around basal obstacles, provides a first approximation for glacier speed. Without better rheological information, we assume that the exponent in the Glen (1955) power law (n) is 3, in which case the exponent in the Weertman (1957) sliding law is $(n + 1)/2 = 2$, indicating that sliding could be proportional to the square of the basal shear stress. Basal shear stress can be approximated by:

$$\boldsymbol{\tau = \rho g h \alpha}$$

where $\boldsymbol{\tau}$ is the basal shear stress, is the density of the rock glacier (typically about 1800 kg m^{-3}, which assumes an approximately 50/50 mixture of interstitial ice and debris (e.g., Wahrhaftig and Cox, 1959, p.403; Haeberli 1985, Table 4; Barsch 1987a, Table 4.2), g is the acceleration due to gravity, h is the thickness of the rock glacier, and $\boldsymbol{\alpha}$ is the slope of the surface (Clark et al., 1998). For our purpose, the precise value of the density is not important if we assume that it is approximately the same in all locations, so estimates of thickness and slope are the only variables that must be determined for each survey station. Slope was determined by the methods described in the previous subsection. Thickness is calculated by determining the likely

position and elevation for each survey station had the rock glacier not overlain the valley. This is accomplished by gathering elevations from the adjacent valley, and then subtracting the elevation recorded at each survey station.

3.6 Other Motion-Based Studies

Because of the limited amount of data on rock glaciers, especially in terms of their motion and internal dynamics, we compare rock glacier motion at El Altar, QDM, and Los Azules with the rates of motion obtained from previous studies that used terrestrial laser scanning and DinSAR (Kane, 2014; Hopkins et al., 2014) to analyze our study landforms. We also compare the rate of motion calculated herein with other similar landforms observed globally using data provided in a broad literature review.

Chapter 4

RESULTS

4.1 Close Range Digital Photogrammetry and Derivatives

4.1.1 El Altar Topography

At El Altar, a total of 784 aerial images were collected and aligned using 10 reference points identified within the images. These aligned photos were used to construct a point cloud of 5.2 million topographic points, from which elevation (Figure 5), and slope models (Figure 6) were derived with 0.25 m ground sample distance. Using the break in slope along the margin of the rock glacier to differentiate a boundary with the surrounding land surface, the rock glacier covers an area of 65,400 m^2 and extends approximately 750 m in length with a maximum width of approximately 210 m that tapers to ca. 100 m at the terminus. Geomorphic analysis of the surface topography indicates two distinct portions of the glacier. The upper portion has an average slope of 13° and 10 transverse lobes extending from the cirque headwall to 210 m down valley. This upper portion of the glacier also contains two elongated furrows that extend up to 225 m on both sides of the lateral margins. The lower half of the glacier has an average slope of 7° and is characterized as hummocky terrain that is depressed several meters below the raised ridge of the terminal margin. Additionally, there are remnant furrows in the lower portion, but they are smoothed and blend into the hummocky terrain. The long axis of the lower portion of the glacier is oriented approximately 12° to the west compared to the upper portion.

4.1.2 QDM Topography

At QDM, a total of 73 aerial images were collected and aligned using automated settings to construct a point cloud of 17,000 topographic points, and to derive subsequent elevation (Figure 7), and slope models with 0.25 m resolution (Figure 8). Using the break in slope of the rock glacier margin with the underlying terrain as a boundary, the rock glacier covers an area of 50,243 m^2 and is approximately 20 m higher in elevation than its surroundings on average. The QDM rock glacier is at an average slope of approximately 18° and contains just two well-defined elongated transverse ridges on the eastern portion that extend approximately 130 m down glacier. QDM flows down valley from a cirque wall to the north at a direction of approximately 120°.

4.1.3 Los Azules Topography

Los Azules presented the most complicated scenario for data collection. The eastern portion of the glacier lacks many obvious glacial landforms and displays poorly organized hummocky terrain. Thus, this study focuses on the western portion of the rock glacier. For the western portion of the rock glacier, a total of 455 aerial images were collected and aligned based on automated settings to construct a point cloud of 58,000 topographic points from which subsequent elevation (Figure 9), and slope models were derived to 0.25 m ground sample distance (Figure 10). Using the break in slope between the glacier and the adjacent terrain as a boundary, it covers an area of 116,963 m2, with a maximum width of ca. 220 m on the westerly portion, tapering to 95 m on the lower southeast portion. This portion of the glacier flows downslope in a southeasterly direction, approximately 140°, with an average slope of approximately 20°. The slope is approximately 40° on the terminal margin. The upper

northwest portion contains a series of 5 elongated furrows that extend approximately 155 m down the glacier. These ridges are significantly less pronounced on the lower portions of the glacier, and this portion significantly resemble the hummocky terrain of the eastern portion of the glacier.

4.2 Motion from repeated GPS surveys

4.2.1 El Altar Motion

Ground motion data recorded at the El Altar rock glacier indicates downslope motion that varies spatially (with distance downslope) and temporally (between measurements), with rates between 0.03 m yr^{-1} and 0.16 m yr^{-1} (Table 3, Figure 11). Three GPS survey stations located on the upper portion of the glacier displayed the fastest movement. Station MO19, located on the terminus of the first and highest of the 10 transverse lobes at an average slope of 2°, moves at an average rate of 0.16 m yr^{-1}. Station MO18, approximately 132 m down the glacier from station MO19 on the ridge of the last well-defined transverse lobe, also displays an average slope of 2° and moves at an average rate of 0.09 m yr^{-1}. The next GPS station downslope, MO09, located where the transverse lobes begin to form an elongated furrow, displays a slope of 13° and moves at an average rate of 0.07 m yr^{-1}. The subsequent 8 GPS stations are located on the lower portion of the glacier and reveal slower movement. Station MO08, located approximately 57 m southwest of MO09 on the ridge of the outermost elongated furrow, displays an average slope of 19° and moves at a yearly average of 0.05 m yr^{-1}. Downslope from station MO08 is primarily hummocky terrain. Southeast of MO08 lies a cluster of 4 stakes, emplaced as a field test to ensure this particular section of the rock glacier was flowing coherently.

Station MO03, the easternmost point on the cluster, is the only stake of the cluster with multi-year (83 months) motion data. Station MO03 is located on an 8° slope and moves at an average rate of 0.08 m yr^{-1}. The remaining three stakes in the cluster also move at 0.07 m yr^{-1} to 0.08 m yr^{-1}. Although the other three stake motions are based on fewer measurements over a short time period, they show reasonable coherence over the small area. The slopes vary widely, however, from 30° at MO02 (westernmost of the cluster) down to 5°at MO04 (southernmost). This indicates that for the purpose of studying the dynamics, these slopes are most likely being calculated too locally and that the local motion is based on averaged slope conditions over a significantly larger area than described in section 3.2. Only station MO03, with the longer time baseline, is used for further statistical analysis.

Station MO10 is located approximately 50 m from MO01, located on a slope of 12° and moves at an average rate of 0.08 m yr^{-1}. The easternmost station on El Altar, MO07, is located on a slope of 18° and moves at an average rate of 0.04 m yr^{-1}. Station MO11 is located at the snout of the rock glacier on a slope of approximately 8° with average stake movement of 0.06 m yr^{-1}.

On El Altar rock glacier, the velocities measured at the stations in the upper portion of the rock glacier are 2 to 5 times greater than those in the lower-elevation portion of the rock glacier (Figure 11). The greatest annual displacement detected occurs at the highest-elevation transverse ridge (the most well-defined transverse ridge, so likely most recently formed due to weathering processes acting for a lesser period of time) at stake MO19, which moves 0.15 m yr^{-1}. The second-fastest motion, recorded at station MO18 on the upper part of the transition between the upper glacier and the lower glacier, moves at a rate of 0.09 m yr^{-1}, which is only slightly faster than

most of the stations in the lower portion of the glacier. The overall pattern of the station velocities suggests a significant amount of compression between the upper part of the glacier and the lower part of the glacier, which is geomorphically compatible with the large moraine-like transverse ridge on which station MO18 is placed, as well as with the smaller lobate transverse ridges above station MO18.

The slowest motion on El Altar is at the terminal margin (station MO07), which moves at 0.03 m yr^{-1}. However, as discussed above, most of the stations on the lower glacier are in the 0.06 m yr^{-1} to 0.08 m yr^{-1}. The slow surface velocity leads to low surface strain rates, probably reflected in the relatively minor amount of surface features in the lower glacier away from the lateral and terminal moraines.

Comparing rate of motion with elevation at all points of El Altar revealed a close correlation with elevation ($R^2 = 0.76$, Figure 12a[5]). However, when MO19 is removed from the correlation as an outlier, as both the highest elevation point and the point of the most rapid rate of motion, the R^2 value drops to insignificance ($R^2 = 0.22$, Figure 12a[5]).

4.2.2 QDM

Ground motion data measured by GPS at three stations placed into the QDM rock glacier indicate downslope motion that varies along the rock glacier from 0.10 m yr^{-1} to 0.26 m yr^{-1} (Table 3, Figure 13). QMRG-6L, located on a crest of what appears to be a remnant transverse ridge, is located on a slope of 22° and is the fastest moving of all three monitoring stakes, moving at an average rate of 0.26 m yr^{-1}. QMRG-5L is the furthest down the glacier, approximately 89 m southeast of QMRG-6L at the crest of the snout on a slope of 18°, moving at a yearly average rate of 0.15 m yr^{-1}. QMRG-7L is the furthest up the glacier, approximately 144 m northwest

of QMRG-6L, located on the border of two slightly different sediment types (one lighter in colour, and one slightly darker and more fine-grained). QMRG-7L is the slowest moving of all three QDM monitoring stakes with average annual motion of 0.10 m yr^{-1} and is located on a slope of 14°.

The pattern of velocities on QDM is more easily characterized, in part because there are only three data points. The pattern of speeds along what may be a central flowline is more typical of a "normal" glacier in having lower speeds at the head and terminus and higher speeds in the middle. In contrast to the surface geomorphic patterns shown on the other rock glaciers in this study, QDM is quite smooth and mostly shows a surface response to glacier motion in the terminal moraine. Local slope at QDM appears to correlate well with rate of motion (R^2 value of 0.97, Figure 14b[8]). However, with three GPS survey stations, this correlation is not statistically significant.

4.2.3 Los Azules

Data from survey stations MAW3, MAW2, MAW1, MAE3, and MAW5 indicate downslope motion that varies along the rock glacier from 0.03 m yr^{-1} to 0.04 m yr^{-1} (Table 4, Figure 15). Analysis of the geomorphology as seen in aerial imagery suggests two different zones, 370 m apart, evident from furrows in the direction of flow that indicate flow from two different accumulation areas, termed east and west herein.

Survey stations on and near MAE2, MAE3, MAE4, and MAE5 flow toward the eastern accumulation zone. MAE4, the stations furthest east, flows into the eastern accumulation zone and is located on the crest of the snout and moves at an average yearly rate of 0.06 m yr^{-1}. Station MAE5 is located approximately 76 m southwest of

MAE4 on the crest of the snout and moves at an average rate of 0.03 m yr^{-1}. Station MAE3, the only stake on the eastern accumulation zone section to be captured by the orthoimagery, located 167 m northwest of MAE5 on hummocky terrain on a slope of 31°, and moves at 0.03 m yr^{-1}. MAE2, located 76 m north of MAE3, moves at an average annual rate of 0.06 m yr^{-1}.

Points on and near stations MAE1, MAW1, MAW2, MAW3, MAW4, and MAW5 flow toward the western accumulation zone. Station MAW5 is located at the snout of the western accumulation zone on a slope of 21° and moves at an average rate of 0.029 m yr^{-1}. MAW1 is located approximately 48 m up the glacier from MAW5 on a slope of 16° and moves at a yearly average rate of 0.04 m yr^{-1}. MAE1, located 67 m northeast of MAW2, moves at a yearly average rate of 0.04 m yr^{-}. MAW3, located 120 m west of MAE1 on a slope of 8°, moves at an average rate of 0.02 m yr^{-}. MAW4, the westernmost of all stakes, moves at a yearly average rate of 0.04 m yr^{-}. Based on the combined GPS data from all stations at Los Azules, slope was found not to be a factor in the rate of motion (R^2 value of 0.081, Figure 14c). Elevation, however, showed a R^2 value of 0.53, so is somewhat correlated with rate of motion (Figure 12c).

4.3 ASTER Slope

An ASTER Global Digital Elevation Model (GDEM) for this study area was obtained to compare and contrast the slope values reported by stitching together close range aerial imagery. Interestingly, the slope models created using the ASTER GDEM were an average of approximately 5° less than the slopes reported by using the aerial imagery. For example, the slope obtained from station MO11 was calculated as 18° from areal imagery (Figure 5), whereas the slope obtained from ASTER at MO11 was

calculated as 14° (Figure 16). At QDM, similar slope differences were reported. For example, the slope obtained from ASTER at QDMRG-7L was calculated as 19° (Figure 17), and the slope obtained from areal imagery at QDMRG-7L was 14° (Figure 8). Additionally, this trend was observed at Los Azules. For example, as seen in Figure 18, the slope observed at MAW3 obtained from ASTER imagery was 5°, and the slope obtained from areal imagery at MAW3 was 8° (Figure 9). Slope values for each station were recorded and then plotted against their associated average yearly movement (Figure 19).

Geometric data extracted from the output models indicate that as reported by the slope models created by the ASTER imagery, the average slope at the upper portion of the El Altar rock glacier is greater (13°) than the lower portion (9°). There is a R^2 value of 0.04 reported when plotted against the yearly average motion.

At the QDM rock glacier, the slopes reported by the ASTER imagery indicate that the QDMRG-5L, QDMRG-6L, and QDMRG-7L stake slopes ranged from 19° to 22°. QDMRG-6L was located on the steepest slope, and QDMRG-7L was located on the most gradual slope. These results are in alignment with the slopes recorded by use of close range aerial imagery. Slope and rate of motion are seen to be very well correlated (R^2 value of 0.98).

Extraction of geometric data obtained from the GDEM at Los Azules indicates a slope that ranges from 5° to 25°. Two additional survey stations, MAW4 and MAE1 through MAE5, (Figure 4) were included in this report to obtain a broader context of how slope affects motion on the Los Azules rock glacier. Station MAW3 is located on the most gradual slope (5°), and MAW1 is located on the steepest slope, 25°.

Chapter 5

DISCUSSION

This study of the El Altar, QDM, and Los Azules rock glaciers, combining centimeter-scale motion data with topographic data and derivatives developed from close range digital photogrammetry, reveal in unprecedented detail the correlations in spatial variation of surface motion of these landforms. By examining the rate of motion in conjunction with detailed topographic data, we are able to distinguish between which glaciers or portion of the glaciers move at velocities typical of an ice-rich form. Data from the survey stations emplaced across each landform, when monitored over time, suggest that parts or all of the three landforms are active, with flow patterns reflecting complex internal dynamics that are distinct in each of the three settings. While visual analyses of the landforms suggested that they had been active recently enough to show surface indications of motion, identifying buried ice is important to know if the rock glaciers are currently active. In two of the three landforms (QDM and Los Azules), buried ice has been identified. Excavations into the terminus of El Altar have yet to identify buried ice (Andres Meglioli, personal communication 2017), though a faster moving upper portion of the rock glacier are potentially indicative of buried ice. Importantly, these findings help inform the appropriate application of the National Glacier Act as it pertains to these three study locales, and also provide a methodology for future monitoring efforts in the region. Additionally, due to the difficulty of accessing this remote terrain, spatial datasets regarding the geometry and topography of these three rock glaciers are especially valuable in this little-studied region.

The internal dynamics of each rock glacier likely differ greatly as a function of the variations in the ways in which these three rock glaciers were formed and/or continue to evolve – the variation in grain size and sediment type, microclimate (aspect, moisture availability, sun exposure), as well as the current and potential new ice content. As such, each glacier will be examined separately.

At El Altar, the appearance of defined transverse lobes and nested elongated furrows on the upper portion of the glacier suggests that the upper portion is significantly more active than the lower portion. A near standstill of the terminal margin (i.e. moving 2 to 5 times slower than the upper section) suggests that the lower portion may be reaching stagnation at its low elevation of 3600 (i.e., warmer microclimate) and away from the headwall (i.e., supply) from which this rock glacier extends. The rate-of-motion observations herein correlate more significantly with elevation than with local slope, implying that increased ice presence at higher elevations is likely playing a role in motion. If movement was simply a result of creep, a stronger correlation with slope would be expected across the entire landform. These observations and interpretations are consistent with previous studies on this landform. DinSAR (Differential Synthetic Aperture Radar Interferometry) data for El Altar, analyzed by Hopkins et al. (2014), identified rates of motion ranging from 60 ± 30 mm yr^{-1}. Kane (2014) estimated that the El Altar rock glacier accretes downvalley at a rate of ~3.5 cm yr^{-1}, as measured by LiDAR scanning in AD 2013 and 2014. These values are consistent with those measured by both GPS and LIDAR in our group's studies, albeit, as reported by this paper, slightly slower than the 85 to 100 mm yr^{-1} observed with the GPS data for the fastest upper portions of the rock glacier.

This difference may be due in part to a lack of DinSAR data in the upper section caused by line of site anomalies not scanned by the satellite altimeter.

El Altar displays a weak correlation between basal shear stress and rate of motion (Figure 20a), indicating that thicker portions of this rock glacier, containing greater slopes, do not necessarily move faster, contrary to the typical behavior of an ice glacier. Although the lower portion of the rock glacier may appear thick (~20 m), it is significantly less active than the upper portion where the rock glacier appears to be only a few meters above the local adjacent bedrock. A 10 m pit excavated laterally into the margin in 2015 revealed no ice or significant meltwater.

In contrast to the apparent lack of ice in the terminus of El Altar, the nearby QDM rock glacier provides an opportunity to examine rate of motion of a rock glacier known to contain ice beneath its terminal margin. Excavation in March 2018 into the margin near station QMRG-6L revealed ~2 m of debris-rich ice. Because QMRG-6L is the lowest-elevation survey station of the three observation locations, it is likely the two colder, higher-elevation stations are also sited above ice. QDM shows a strong correlation between slope and rate of motion (R^2 value of 0.97) further supporting the possibility of consistent basal ice throughout the landform. Likewise, there was a strong correlation between basal shear stress and rate of motion (Figure 20b), typical of an ice-rich landform in which flow downslope is a result of gravitational driving stress (a function of slope and thickness). QDM elevation and rate of motion do not correlate well (i.e., the fastest moving stake is along the steeper sloped QMRG-5L in the middle of the landform). It is important to note, however, that, though strong, these correlations result from data gathered at three survey stations. Further work, especially

more survey stations, would be needed at QDM to make these results statistically significant and scientifically reliable.

Of the three study landforms, the Los Azules rock glacier is the slowest, moving at a rate of 0.04 m yr^{-1}, approximately 5 times slower than the fastest moving benchmarks at El Altar. These slow rates of motion are similar to that reported by Kane (2014), who reported an average yearly displacement of approximately 0.045 m yr^{-1}. This value was thought to have been exaggerated by small slope failures and boulder motion, but is on the same scale as the GPS-observed motion reported herein. Los Azules is a complex landform, likely developed as a composite sequence of flows that accumulate on and flow to the southwest that faces into the valley with an axis to the southeast. The variations in flow direction observed at the benchmarks (Figure 15) suggests a lack of self-organization of the landform into a single flow direction. This variation in direction between flow from the cirque and that of the underlying valley may inhibit organized transport, possibly contributing to slow movement. The average slope of Los Azules (19°) is comparable to those of El Altar and QDM (21° and 18°, respectively), so slope differences do not explain the differences in dynamics. Despite the slow motion of Los Azules, excavations in both AD 2014 and 2018 exposed laterally continuous layers of ice along the southwest margin within 4 meters of the surface.

Interestingly, a comparison between of the rates of motion of these three rock glaciers to a global population of 57 rock glaciers identified from a literature review (Table 5), indicates that the study glaciers move approximately 14 times slower than the average of the global population (i.e., 1.14 m yr^{-1} global average rate of motion

compared to the average motion observed at benchmarks at the 3 rock glaciers of this study at 0.08 m yr^{-1}).

We recognize that our results may be affected by the relatively short period of record, as a decade of glacier monitoring is still a snapshot of the conditions under which it exists. Ice presence in glacial landforms should be examined on a long-term, ongoing basis, because small variations in surface energy balance may result in large changes in ice distribution (Osterkamp and Romanovsky, 1999). If it is found that certain locales on a rock glacier contain ice, this may not indicate ice content in other portions of the glacier. Thus, future work that further identifies properties of landforms that are indicative of subsurface ice could also prove useful and applicable to ascertaining activity of rock glaciers in our study area. This research is essential to ensure accordance with the National Glacier Act, which aims to preserve water as a critical resource.

Chapter 6

CONCLUSION

All three rock glaciers studied as part of this thesis show motion and are thus inherently active to varying degrees. However, as seen by Table 5, these rock glaciers move slowly compared to a global population of rock glaciers developed from a literature review. These low velocities suggest a small percentage of ice content imbedded within the debris of these rock glaciers. Because of the location of these study glaciers, their water content is viewed as long term water source.

Because there are few quick processes for weathering of Dry Andes rock glaciers, evaluation of the surface topography and velocities in this thesis provide critical insights for guiding further analyses that can focus on the distribution of ice and volume. By monitoring the movement of strategically placed survey stations and coupling that information with topographic data and simple assumptions about ice flow, we are able to estimate which rock glaciers, or portions of the three rock glaciers studied, likely contain ice. However, because ice is not visible on the surface of the rock glaciers, trenches are required to confirm or deny the presence and percentage of ice in these rock glaciers. Such trenching requires bringing heavy machinery into this terrain, which in turn entails significant expense and potential danger to equipment and its operators. However, continuous monitoring of rock glaciers in this area has the potential of limiting this need by improving our ability to accurately predict ice content based on physiography and motion.

FIGURES

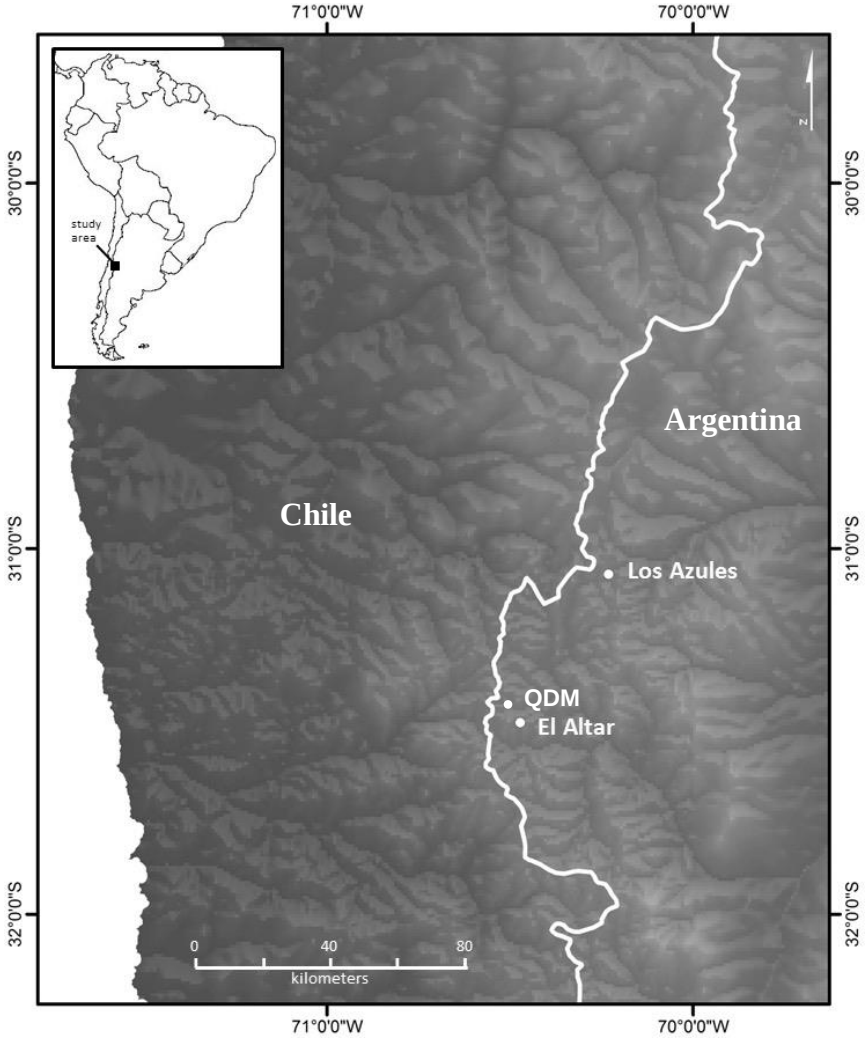

Figure 1 Locations of El Altar and Los Azules study site which are located in the High Andes in Argentina in close proximity to the Chilean border Specifically, El Altar and QDM are located at 31° 28′ S 70° 31′ W, and Los Azules is at 31° 05′ S 70° 14′ W.

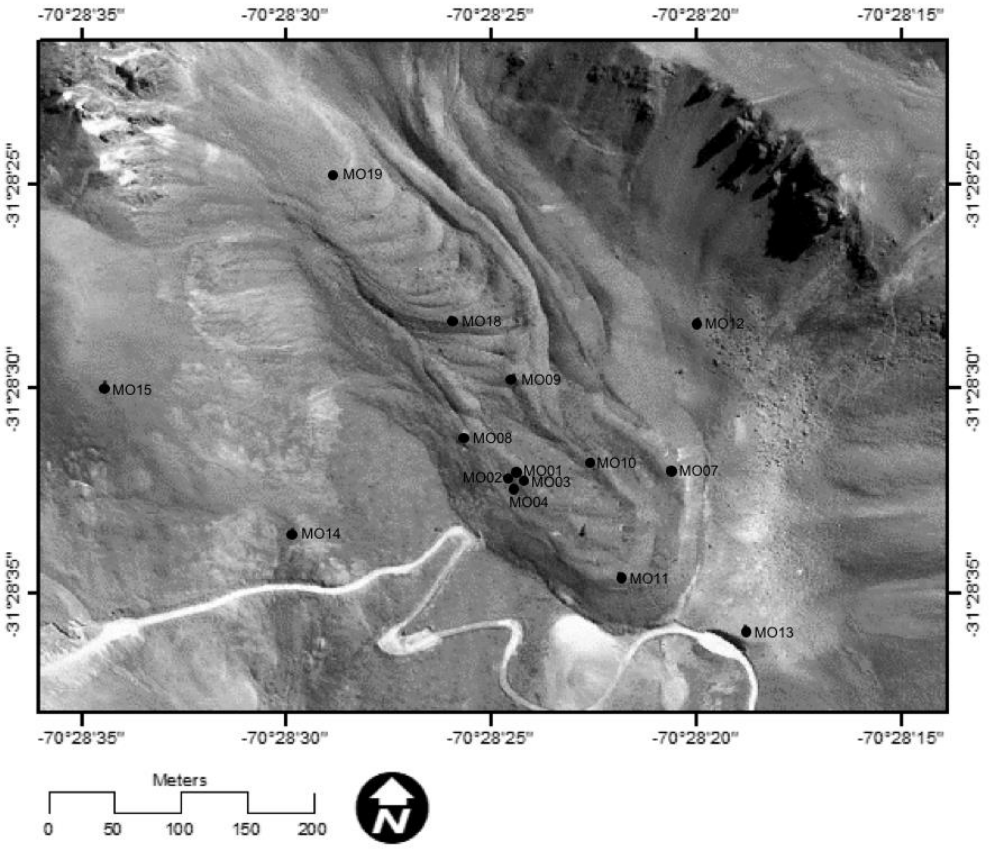

Figure 2 El Altar rock glacier obtained from Digital Globe on 3/30/2010 from Google Earth Pro with locations of 11 motion-monitoring stakes and 4 off-glacier control stakes (MO15, MO14, MO13, and MO12) marked by labelled dots. In the cluster of 4 stakes (MO01 through MO04), only MO03 is used for statistical purposes because it was measured over the longest period: 83 months. The other 3 stakes in that cluster are displayed in Appendix A but are not included in statistical analysis.

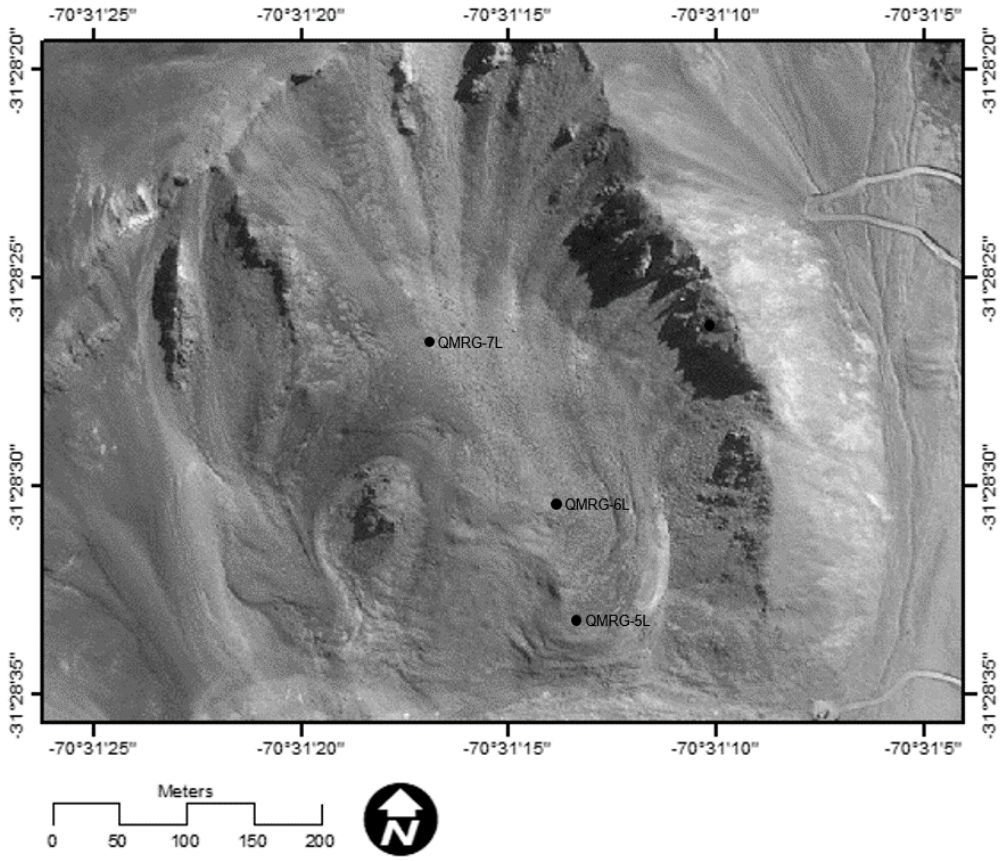

Figure 3 QDM rock glacier obtained from Digital Globe on 3/30/2010 from Google Earth Pro with locations of three motion-monitoring stakes marked by labelled dots. The stakes were placed upglacier, midglacier, and near-terminus along an estimated central flowline based on the surface topography.

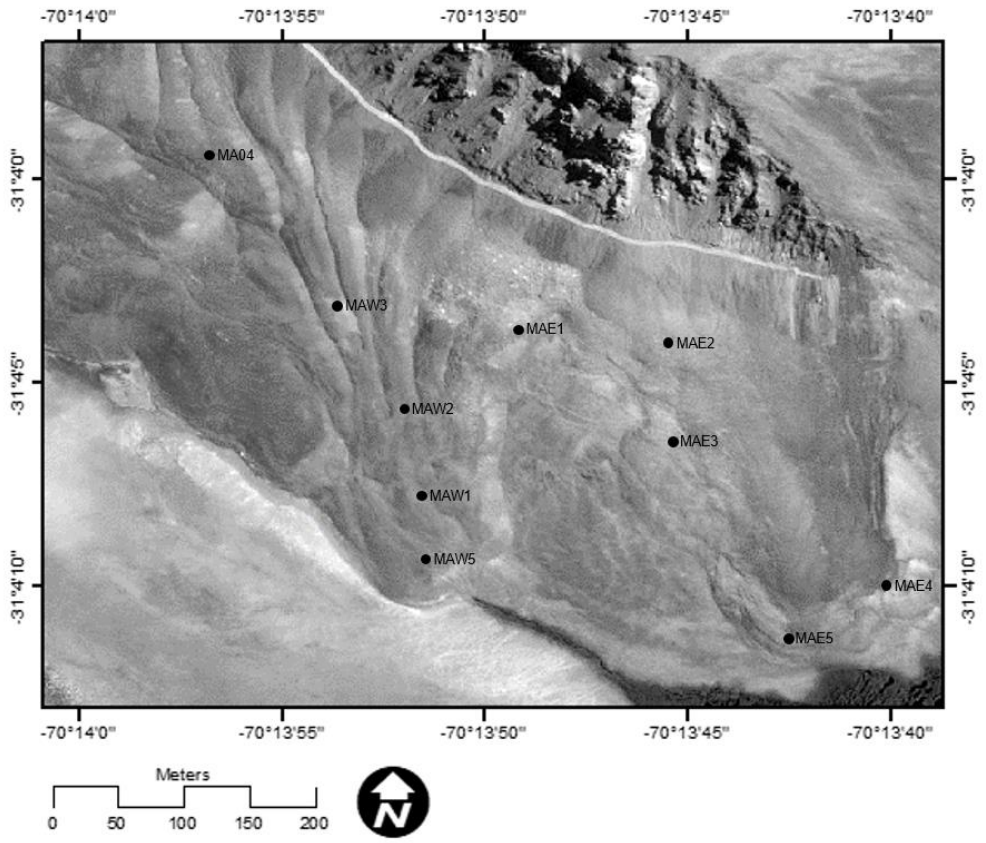

Figure 4 Los Azules rock glacier obtained from Digital Globe on 2/15/2004 from Google Earth Pro with locations of 10 motion-monitoring stakes marked by labelled dots. Motion from stakes MAW3, MAW2, MAW1, MAE3, and MAW5 captured by the orthoimagery, and the additional 5 stakes examined using ASTER imagery. The road, visible as a light curve in the upper part of the image, constructed just above the estimated position of the glacier.

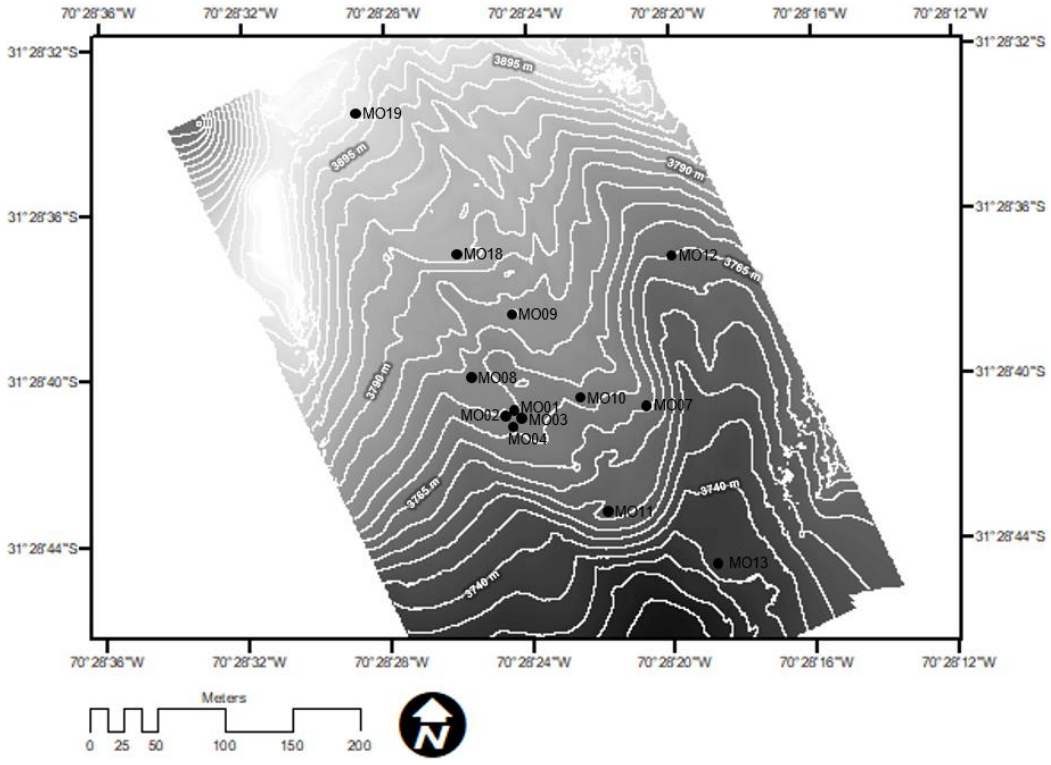

Figure 5 Digital elevation model (DEM) of El Altar rock glacier rendered from stitching areal images captured in March, 2017 using close-range digital photogrammetry survey methods. Stake locations labeled and depicted with points and the image displayed with 5 m contour intervals. The glacier has a general trend of decreasing elevation down glacier towards its tongue.

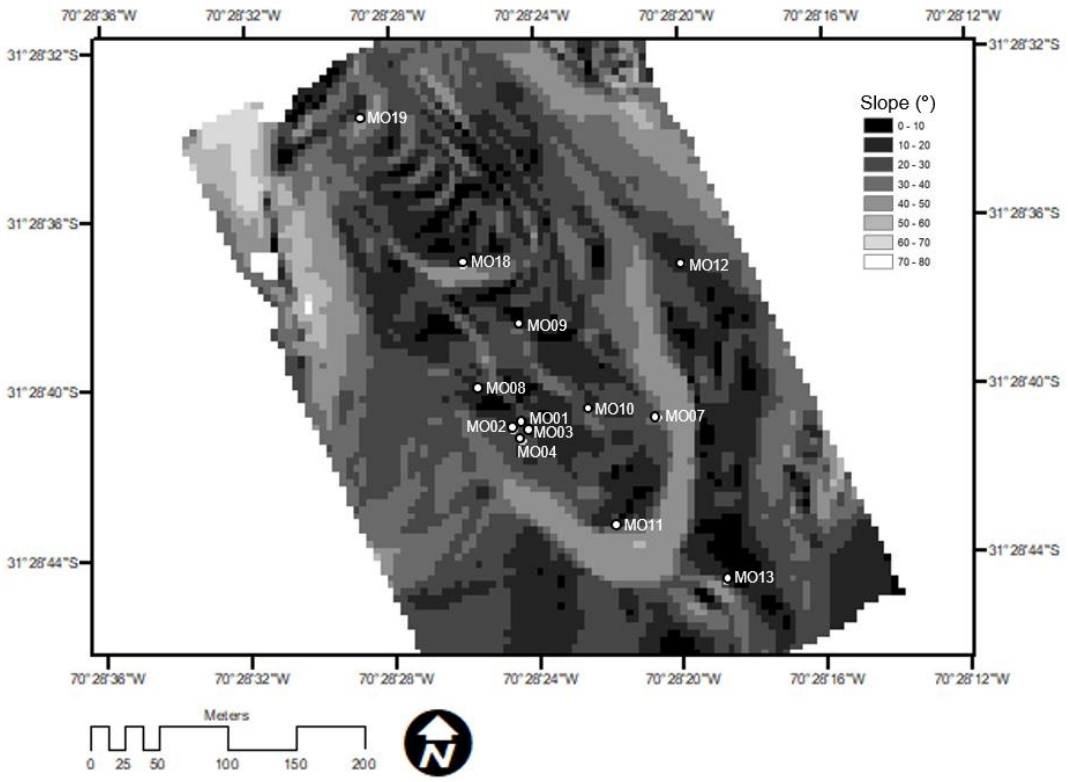

Figure 6 A 5m x 5m slope raster of El Altar rock glacier displays an average slope of approximately 32° on the upper transverse lobes. The flatter lower portion has a slope of approximately 15°.

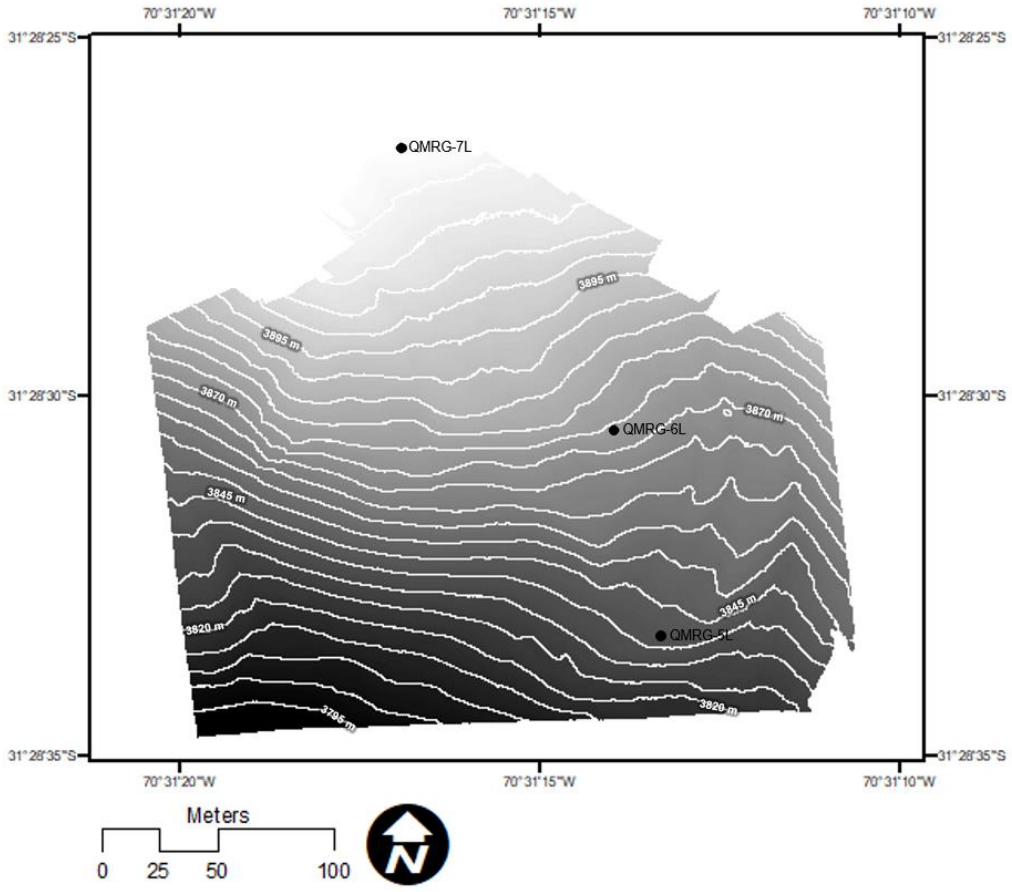

Figure 7 Digital elevation model (DEM) of QDM rock glacier rendered from stitching areal images captured in March 2017 using close-range digital photogrammetry survey methods. Stake locations labeled and depicted with points and the image displayed with 5 m contour intervals. The glacier has a general trend of decreasing elevation down glacier towards its tongue.

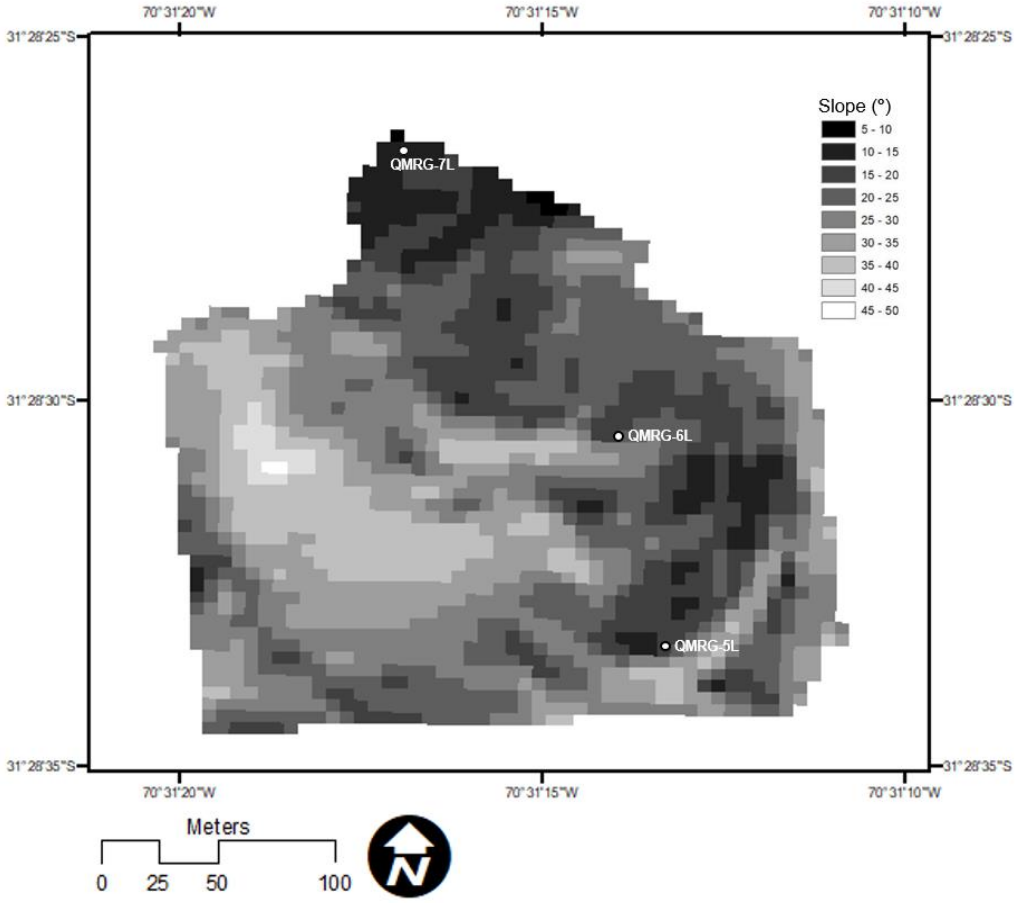

Figure 8 A 5m x 5m slope raster of QDM rock glacier. QDMRG-7L is located on a slope of 14°, QDMRG-6L is located on a slope of 22°, and QDMRG-5L is located on a slope of 18°.

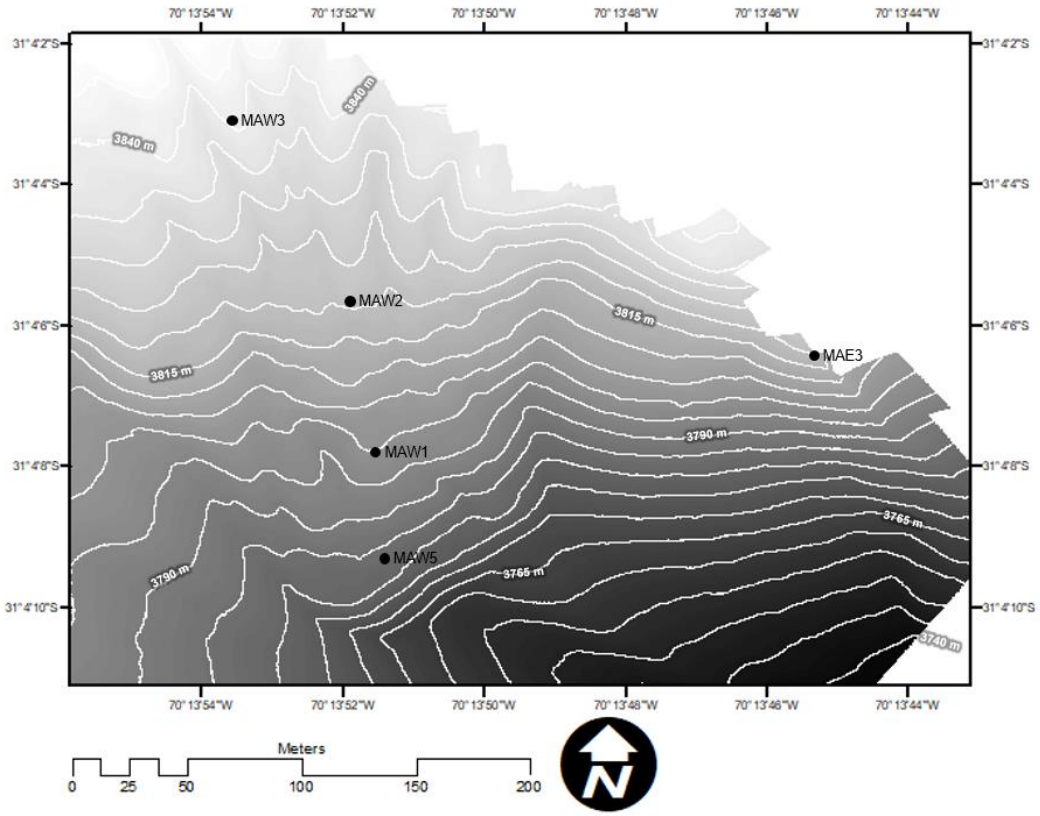

Figure 9 Digital elevation model (DEM) of Los Azules rock glacier rendered from stitching areal images captured in March 2017 using close-range digital photogrammetry survey methods. Stake locations labeled and depicted with points and the image displayed with 5 m contour intervals. The glacier has a general trend of decreasing elevation down glacier towards its tongue.

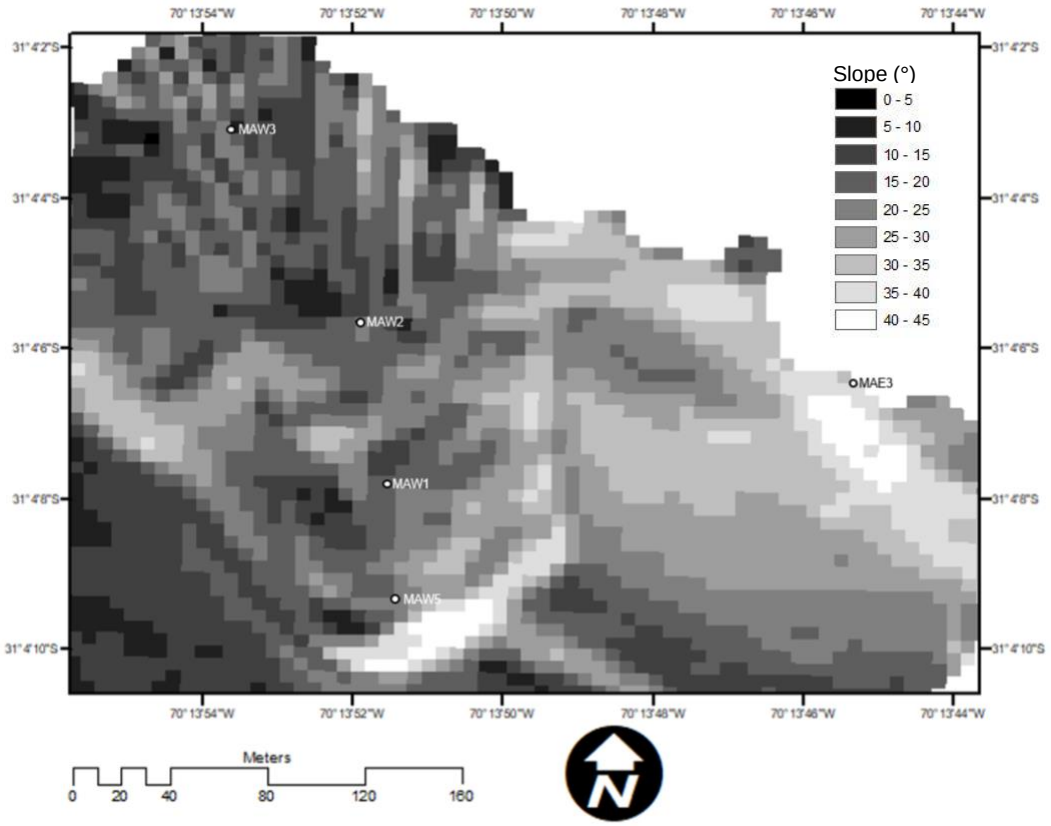

Figure 10 A 5m x 5m slope of Los Azules rock glacier. MAW3 is located on the most gradual slope (8°), and MAE3 is located on the steepest slope (31°). The remaining stakes are located on a slope ranging from 16° to 21°.

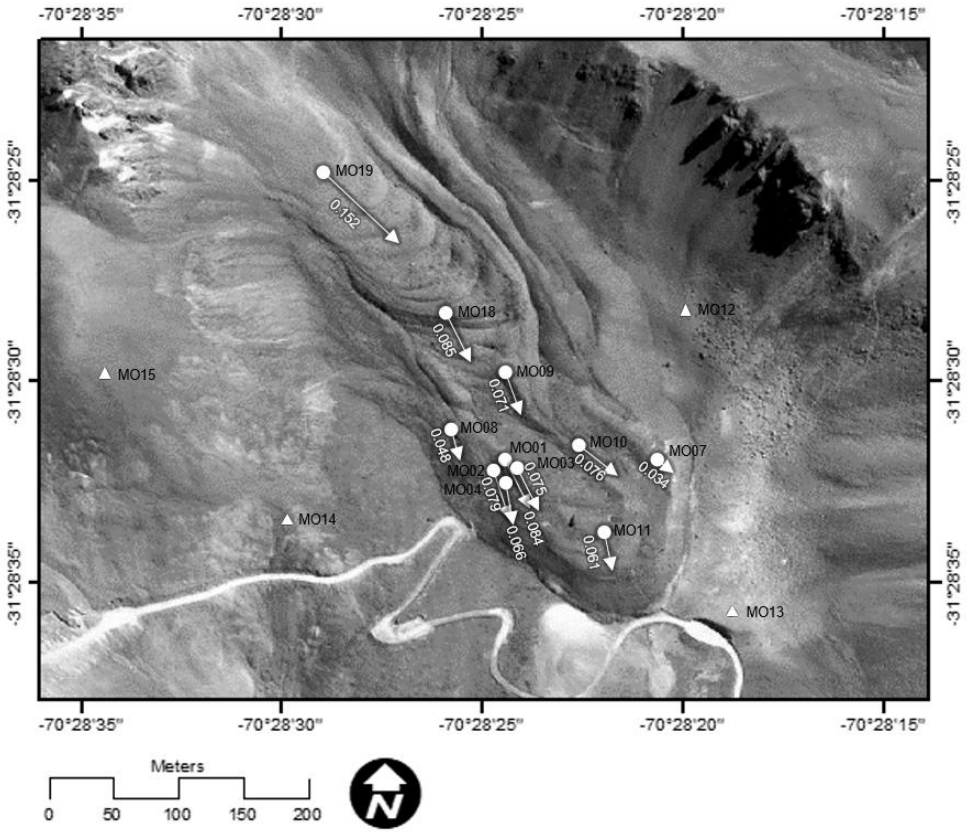

Figure 11 El Altar rock glacier motion vectors and associated speeds in m yr^{-1}. Image obtained from Digital Globe on 3/30/2010 from Google Earth Pro. Control points which recorded negligible movement are labeled with triangles.

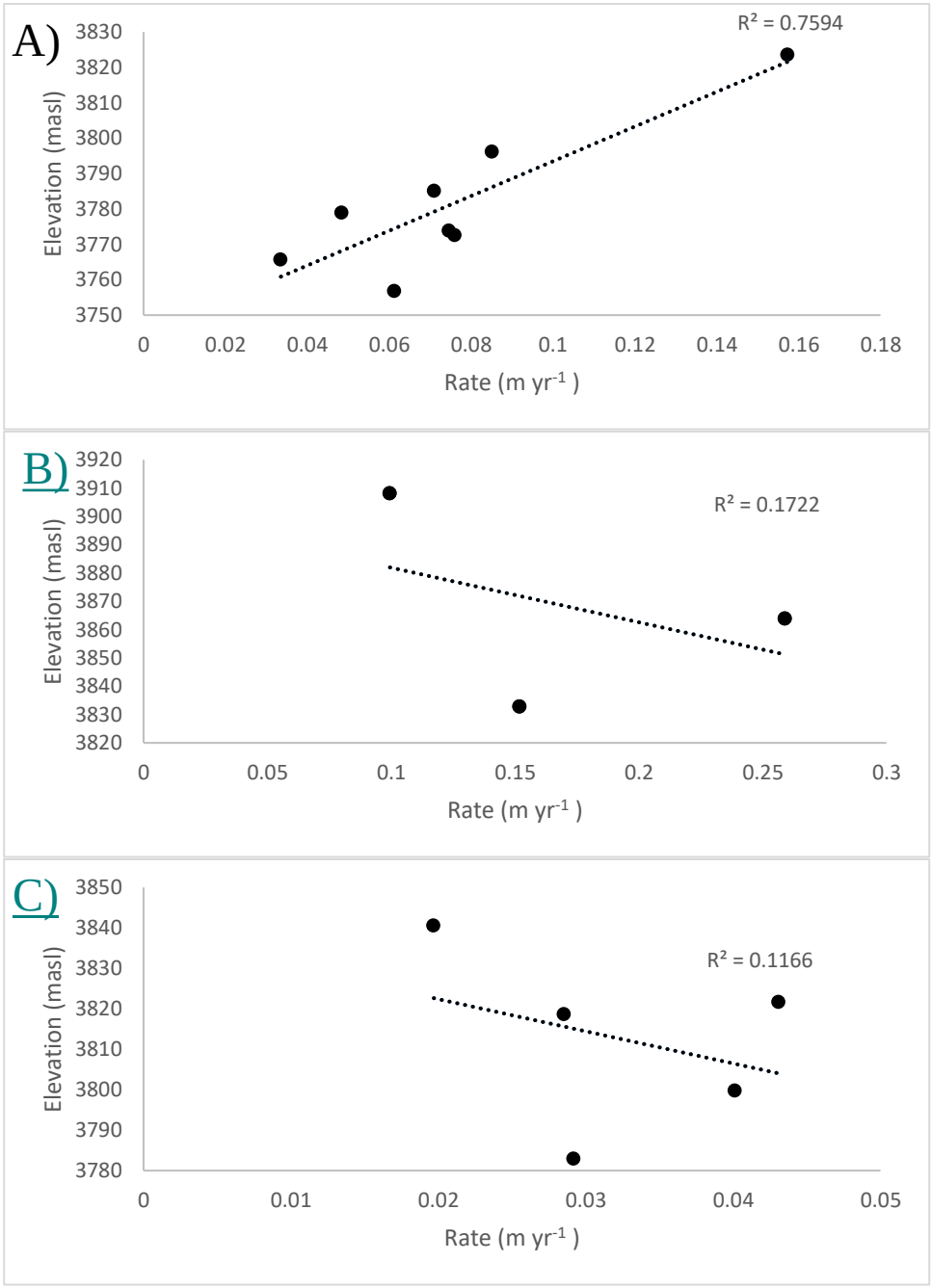

Figure 12 Comparison of rate of motion reported in m yr^{-1} with elevation reported in masl obtained from the DEM created by stitching aerial imagery. A) El Altar rock glacier; B) QDM rock glacier; C) Los Azules rock glacier.

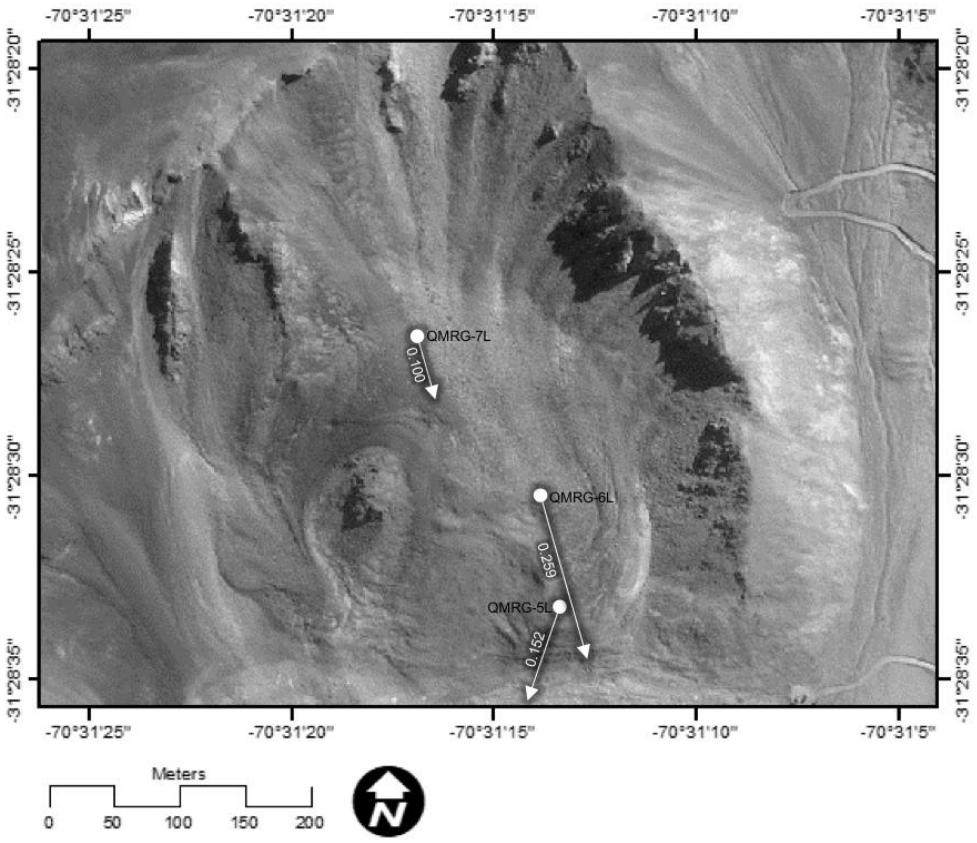

Figure 13 QDM rock glacier motion vectors and associated speeds in m yr^{-1}. Image obtained from Digital Globe on 3/30/2010 from Google Earth Pro and motion data gathered from RTK GPS. QMRG-6L is centermost stake and the fastest moving, and QMRG-7L is the uppermost and slowest moving of the stakes examined.

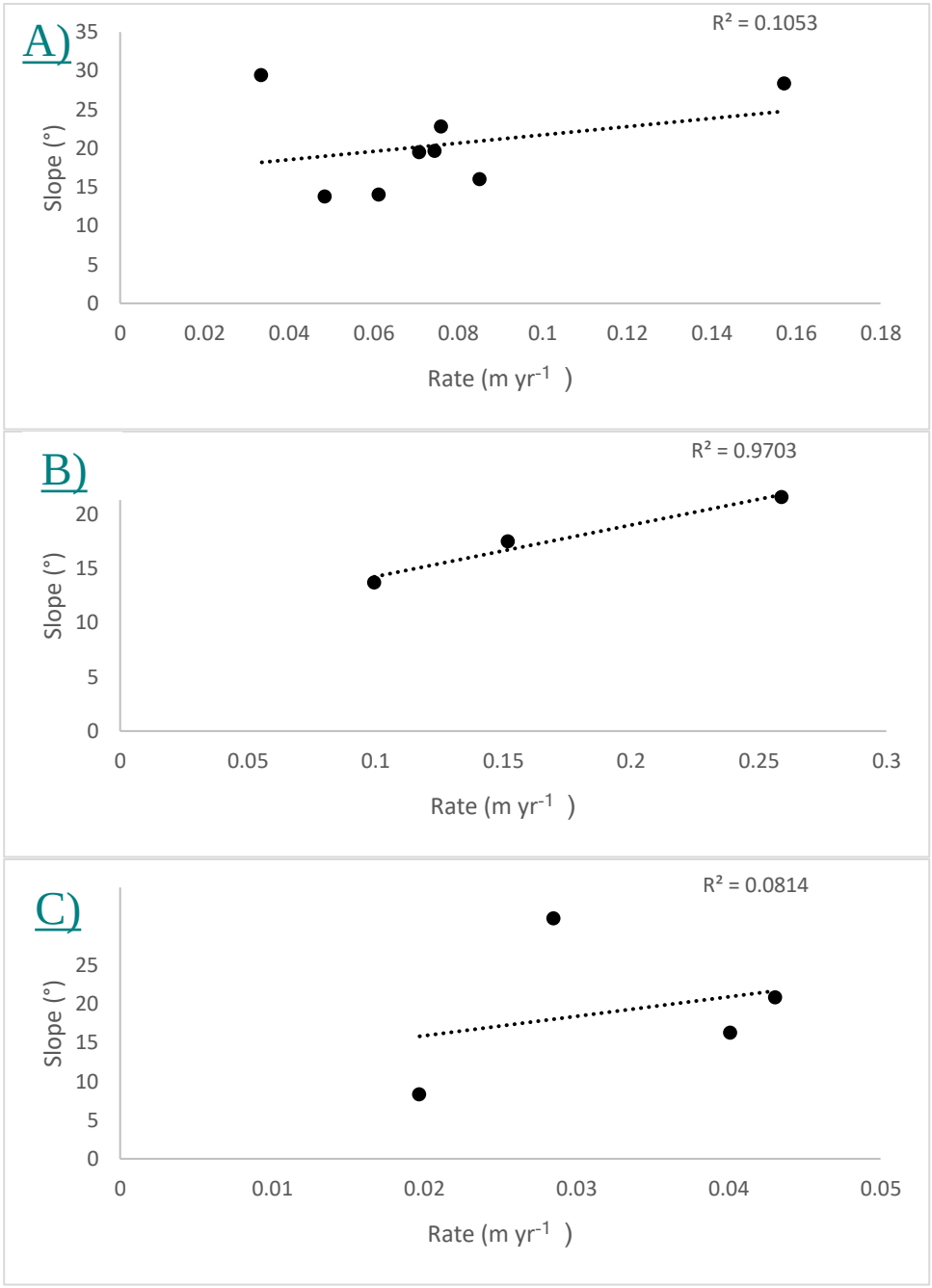

Figure 14 Comparison of rate of motion reported in m yr^{-1} with slope reported in degrees obtained from the slope models created by stitching aerial imagery. A) El Altar rock glacier; B) QDM rock glacier; C) Los Azules rock glacier.

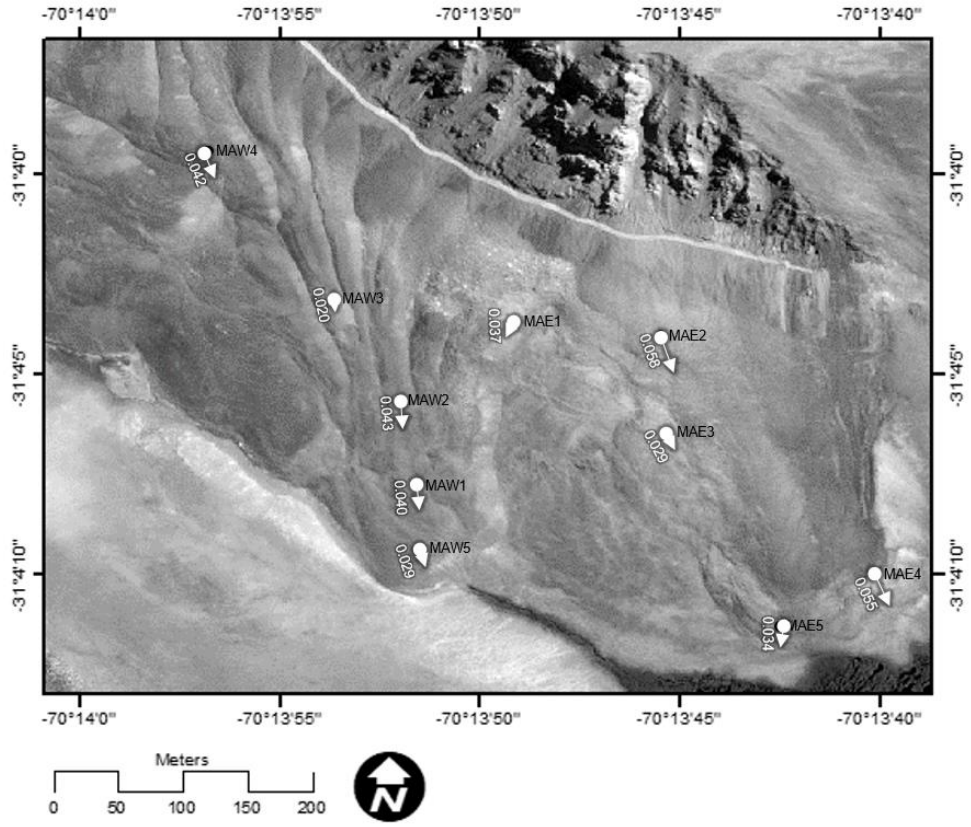

Figure 15 Los Azules rock glacier motion vectors and associated speeds in m yr^{-1}. Image obtained from Digital Globe on 2/15/2004 from Google Earth Pro. All stakes observed move at a significantly slower rate than El Altar and QDM rock glaciers. The fastest moving stake MAE2, which is located on the uppermost portion of the rock glacier flowing to the eastern accumulation zone. The slowest moving stake is MAW3, located on the peak of a transverse ridge flowing to the western accumulation zone.

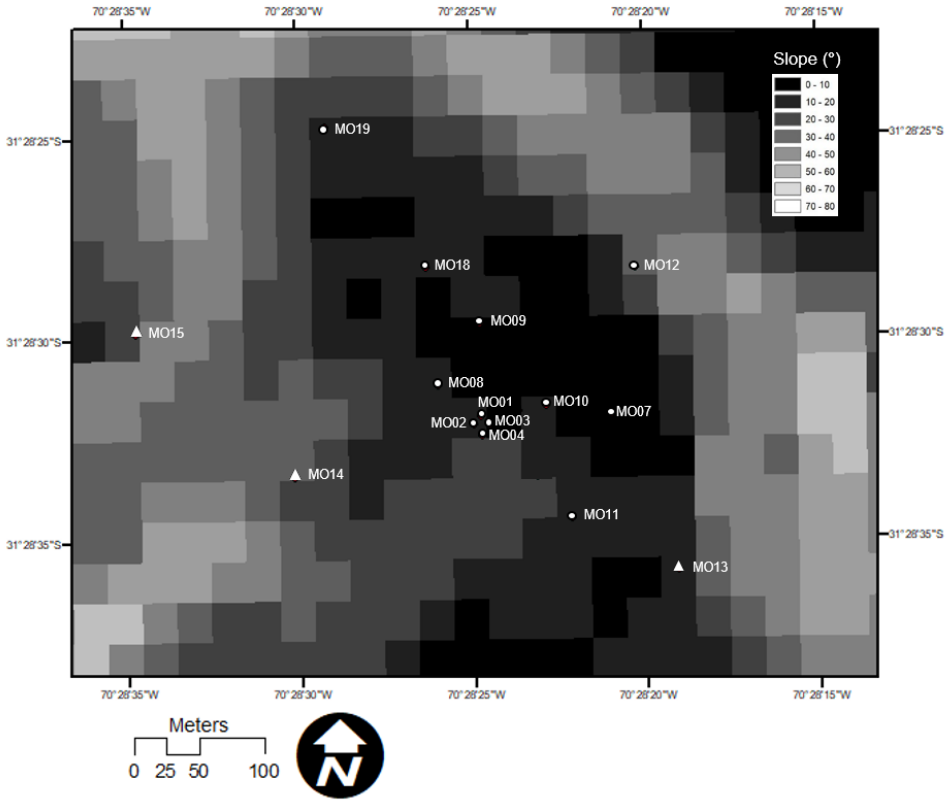

Figure 16 A slope model of the El Altar rock glacier created by using ASTER imagery. All stakes on glacier fall within a slope range of 0°-20°. MO19 is located on the steepest slope (13°), and MO07 is located on the most gradual slope (7°).

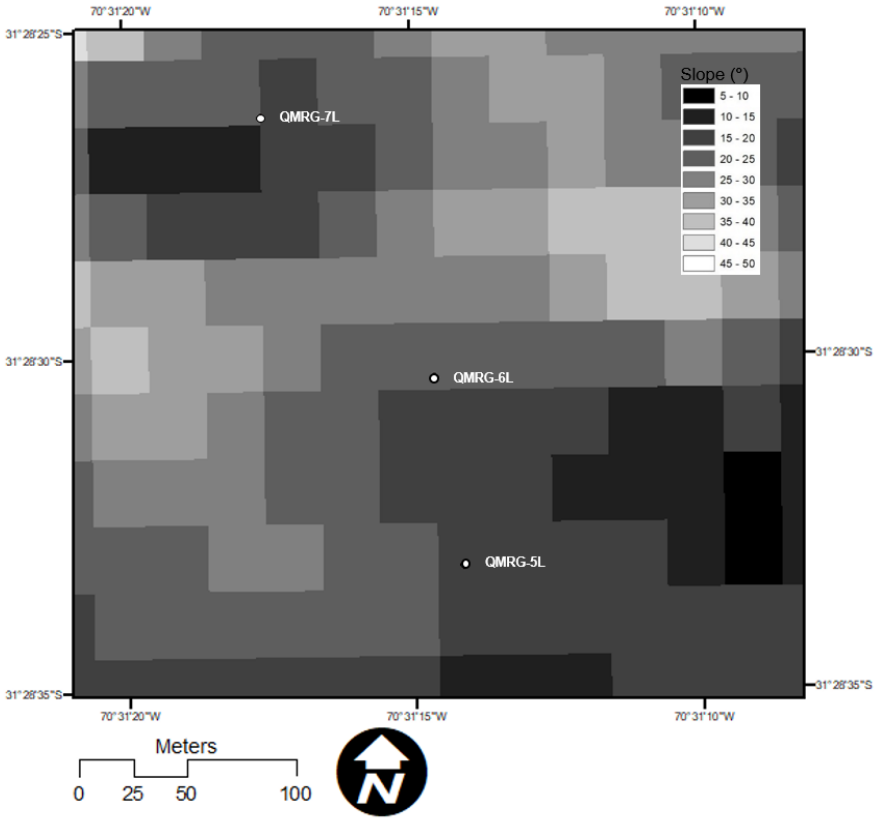

Figure 17 A slope model of the QDM rock glacier created by using ASTER imagery. QMRG-6L is located on the steepest slope (22°) and QMRG-7L is located on the most gradual slope (19°).

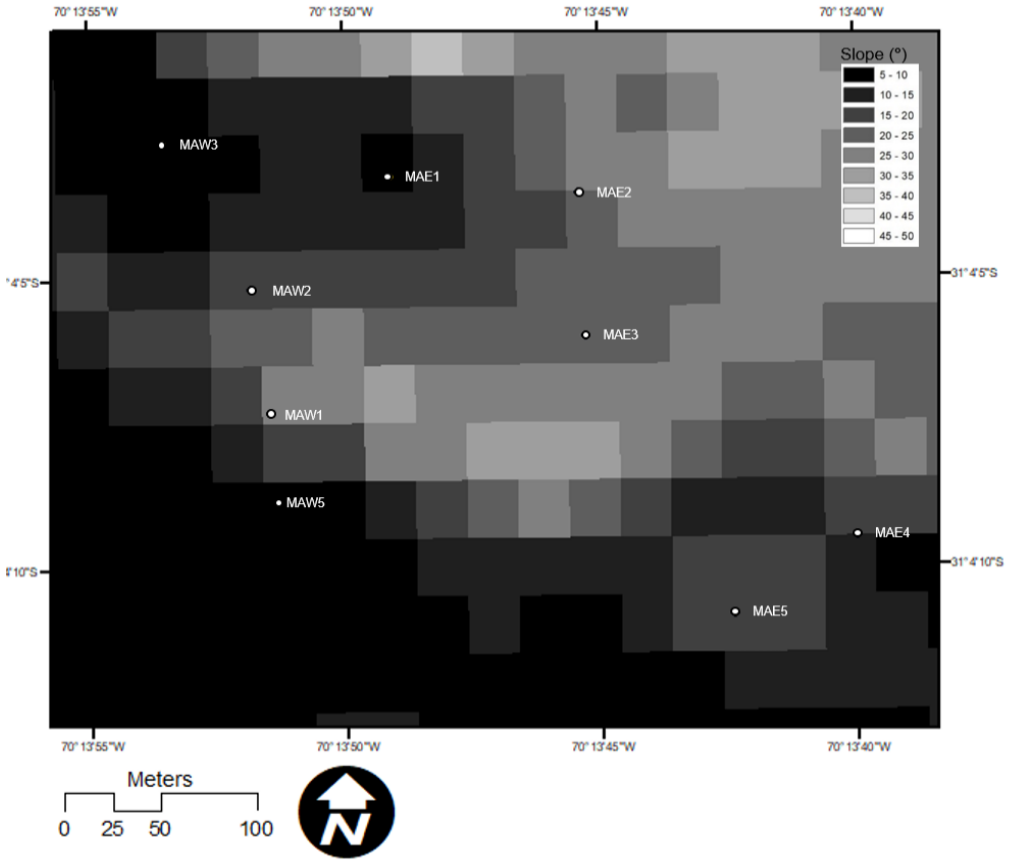

Figure 18 A slope model of the Los Azules rock glacier created by using ASTER imagery. The upper and tongue portion of the rock glacier contain the most gradual slopes (~5°-10°), whereas the center portion contains the steepest slopes (20°-35°).

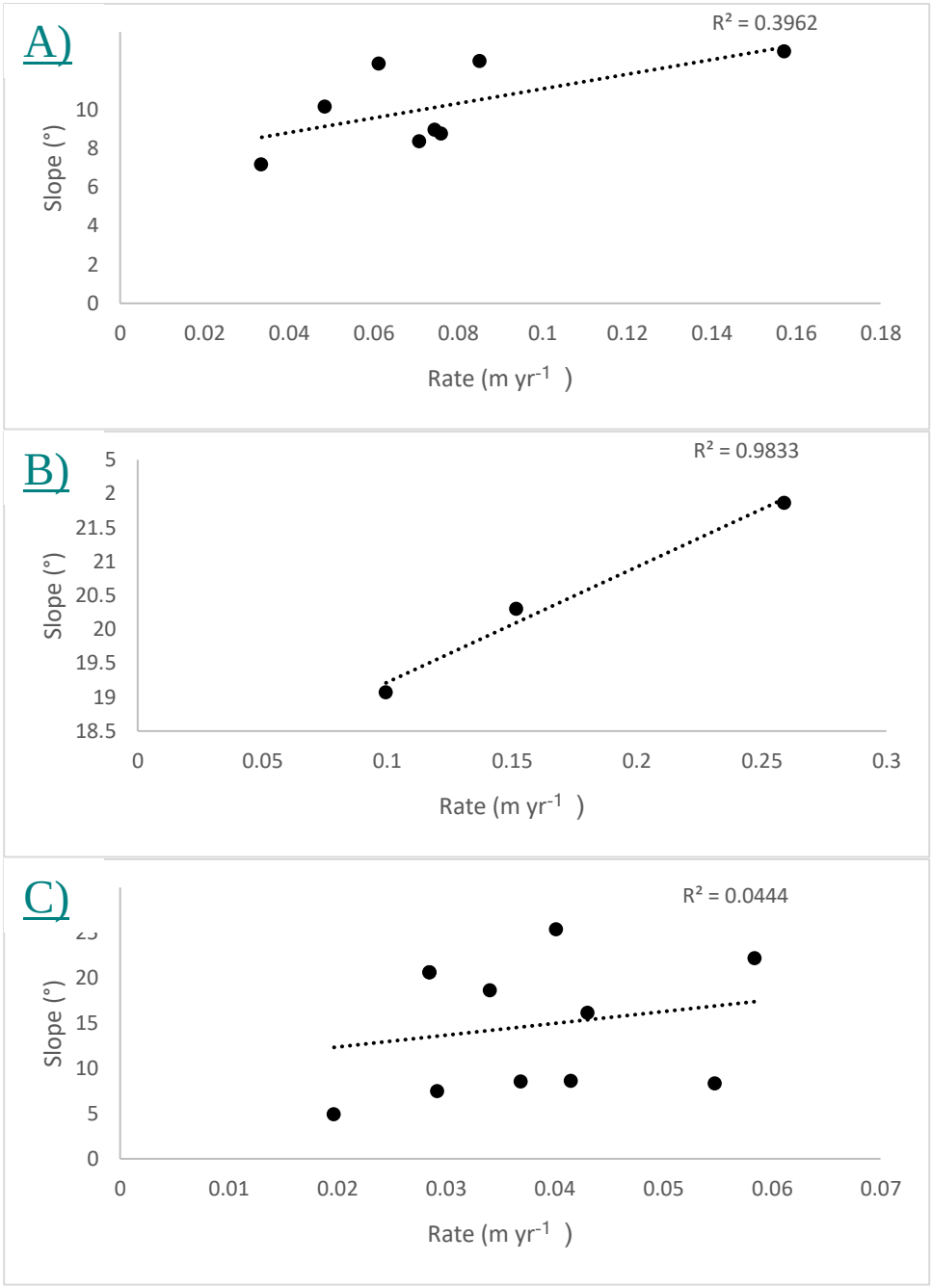

Figure 19 Comparison of rate of motion reported in m yr^{-1} with slope reported in degrees obtained from the slope models created by obtaining ASTER imagery. A) El Altar rock glacier; B) QDM rock glacier; C) Los Azules rock glacier.

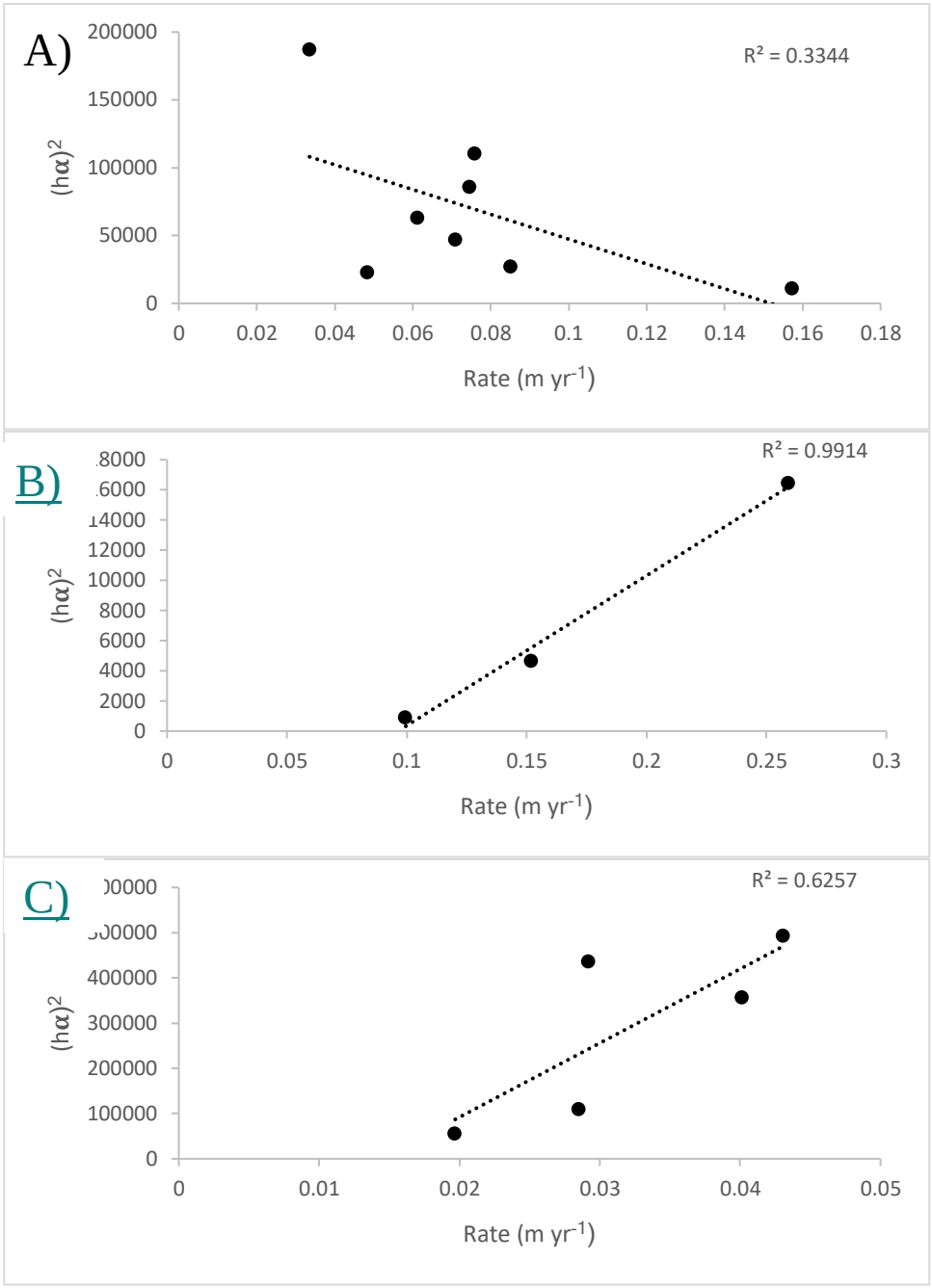

Figure 20 Comparison of rate of motion reported in m yr^{-1} with $(h\boldsymbol{\alpha})^2$ where h is the thickness of the rock glacier obtained from subtracting stake elevations with adjacent valley elevations, and **α** is the slope of the stake obtained from the slope models created from stitching aerial imagery. A) El Altar rock glacier; B) QDM rock glacier; C) Los Azules rock glacier.

TABLES

Table 1 Station numbers and the dates that RTK GPS data were collected for all locations at the El Altar and QDM study areas.

Station Number	Date (month/year)									
	05/10	12/10	04/11	12/11	04/12	12/12	04/13	02/14	03/15	04/17
MO01	•	•								
MO02	•	•								
MO03	•	•	•	•	•	•	•	•	•	•
MO04	•	•								
MO07	•	•	•	•	•	•	•	•	•	•
MO08	•	•	•	•	•	•	•	•	•	•
MO09	•	•	•	•	•	•	•	•	•	•
MO10	•	•	•	•	•	•	•	•	•	•
MO11	•	•	•	•	•	•	•	•	•	•
MO18			•	•	•	•	•	•	•	•
MO19			•	•	•	•	•	•	•	•
QMRG5L						•	•	•	•	•
QMRG6L						•	•	•	•	•
QMRG7L						•	•	•	•	•

Table 2 Station numbers and the dates that RTK GPS data were collected for all locations at the Los Azules study area.

Station Number	Date (month/year)							
	05/11	12/11	01/12	04/12	12/12	03/13	02/14	03/17
MAE1	•	•	•	•	•	•	•	•
MAE2	•	•	•	•	•	•	•	•
MAE3	•	•	•	•	•	•	•	•
MAE4	•	•	•	•	•	•	•	•
MAE5	•	•	•	•	•	•	•	•
MAW1	•	•	•	•	•	•	•	•
MAW2	•	•	•	•	•	•	•	•
MAW3	•	•	•	•	•	•	•	•
MAW5	•	•	•	•	•			

Table 3 El Altar and QDM station numbers and their associated bearing, distance, and elevation change for all recorded dates.

	Date (month/year)																													
	05/10–12/10			01/10–04/11			04/11–12/11			12/11–04/12			04/12–12/12			12/12–04/13			04/13–02/14			02/14-03/15			03/15–04/17		
	Bearing	Distance	z	Bearing	Distance	z	Bearing	Distance	z	Bearing	Distance	z	Bearing	Distance	z	Bearing	Distance	z	Bearing	Distance	z	Bearing	Distance	z	Bearing	Distance	z
MO01	26.565	0.049	-0.006																								
MO02	17.650	0.046	-0.013																								
MO03	25.560	0.051	-0.013	34.287	0.013	-0.013	29.745	0.052	-0.002	24.677	0.020	-0.006	25.253	0.059	-0.011	26.565	0.018	-0.006	36.690	0.064	0.013	26.906	0.075	-0.021	22.457	0.162	-0.121
MO04	10.457	0.059	-0.023																								
MO07	45.000	0.013	-0.013	65.556	0.006	-0.007	54.293	0.020	-0.005	34.287	0.013	-0.008	35.838	0.022	-0.013	59.036	0.006	-0.010	50.194	0.031	0.015	53.842	0.032	-0.017	53.673	0.084	-0.069
MO08	8.130	0.035	-0.026	9.462	0.006	-0.003	16.557	0.039	-0.001	18.435	0.003	-0.030	14.676	0.043	0.006	24.775	0.014	-0.005	0.051	21.325	0.005	0.032	21.240	-0.024	9.554	0.102	-0.062
MO09	16.809	0.050	-0.017	8.746	0.013	-0.010	17.784	0.056	-0.004	31.430	0.011	-0.029	19.026	0.061	0.004	11.310	0.015	-0.008	29.638	0.067	0.001	16.858	0.069	-0.026	16.164	0.144	-0.063
MO10	33.690	0.004	-0.015	30.174	0.025	-0.008	30.964	0.058	-0.014	41.055	0.021	-0.019	27.408	0.061	-0.009	34.380	0.023	-0.005	37.807	0.073	0.008	29.396	0.081	-0.038	31.566	0.180	-0.073
MO11	16.699	0.037	-0.018	7.853	0.015	-0.010	7.125	0.036	-0.010	10.305	0.028	-0.011	11.004	0.037	-0.033	12.529	0.018	-0.005	13.449	0.047	0.000	11.889	0.058	-0.020	10.448	0.143	-0.097
MO12	45.000	0.005	-0.004	54.462	0.004	-0.007	45.000	0.003	0.004	45.000	0.003	0.005	36.870	0.005	-0.009	45.000	0.003	-0.006	45.000	0.004	0.022	#DIV/0!	0.003	0.013	54.462	0.009	-0.027
MO18							22.087	0.074	-0.005	43.363	0.025	-0.019	24.717	0.069	0.004	22.620	0.026	-0.018	31.651	0.086	-0.016	23.772	0.092	-0.026	24.532	0.214	-0.055
MO19							45.000	0.120	-0.035	51.483	0.063	-0.005	46.081	0.112	-0.051	51.009	0.054	-0.023	49.899	0.149	-0.026	45.719	0.169	-0.083	46.874	0.389	-0.115
QMRG-5L													19.440	0.090	-0.048	20.283	0.049	-0.018	21.146	0.114	-0.081	19.026	0.153	-0.064	18.846	0.353	-0.152
QMRG-6L													15.796	0.158	-0.085	15.852	0.084	-0.037	15.599	0.205	-0.096	16.066	0.260	-0.129	15.357	0.589	-0.279
QMRG-7L													18.712	0.065	-0.032	13.570	0.030	-0.007	15.068	0.081	-0.056	15.005	0.100	-0.030	15.482	0.221	-0.056

Table 4 Los Azules station numbers and their associated bearing, distance, and elevation change for all recorded dates.

	Date (month/year)																					
	05/11 – 01/12			01/12 – 04/12			04/12 – 12/12			12/12 – 03/13			03/13 – 02/14			02/14 – 03/17					
	Bearing	Distance	Z	Bearing	Distance	Z	Bearing	Distance	Z	Bearing	Distance	Z	Bearing	Distance	Z	Bearing	Distance	Z	Bearing	Distance	Z
MAE3	168.990	0.010	-0.011	105.255	0.011	-0.004	159.775	0.020	-0.011	139.399	0.009	-0.007	160.710	0.021	-0.014	140.349	0.094	-0.079			
MAW1	182.386	0.024	-0.008	161.565	0.006	0.002	171.870	0.028	-0.010	169.695	0.011	-0.003	168.111	0.039	0.010	174.971	0.125	-0.065			
MAW2	184.236	0.027	-0.007	164.055	0.007	0.003	183.661	0.031	-0.009	153.435	0.011	-0.011	173.047	0.041	0.024	175.700	0.133	-0.047			
MAW3	208.565	0.011	-0.002	168.690	0.005	-0.001	188.130	0.014	0.004	135.000	0.004	-0.005	164.476	0.019	0.021	172.528	0.062	-0.013			
MAW5	182.846	0.017	-0.007	153.435	0.004	0.004	183.740	0.026	-0.004												

Table 5 Rock glacier movement in locations around the world along with associated region, location, and elevation. Movement data given in m yr^{-1}.

Reference	Sample	Region	Latitude	Longitude	Elevation	Rate (m/year)
Delaloye et al., 2009	Lauritchard	Southwestern Alps(France)	45°01'N	06°24'E	2424-2644	1.03
	Mille	Western Swiss Alps (Valais)	46°01'N	07°12E	2340-2430	0.05
	Aget-Rogneux	Western Swiss Alps (Valais)	46°01'N	07° 14E	2810-2890	0.2
	Mont-Gelé B	Western Swiss Alps (Valais)	46°06'N	07° 17E	2600-2740	1.2
	Mont-Gelé C	Western Swiss Alps (Valais)	46°06'N	07° 17E	2620-2820	0.22
	Becs-de-Bosson/Valchy	Western Swiss Alps (Valais)	46° 10'N	07°31'E	2610-2850	0.97
	Furggentälli/Gemmi	Northwestern Swiss Alps	46°24'N	07°38E	2450-2650	3.08
	HuHH1	Western Swiss Alps (Valais)	46° 11'N	07°43E	2630-2780	1.26
	HuHH3	Western Swiss Alps (Valais)	46° 11'N	07°43E	2515-2650	1.78
	Büz North (Trais Fluors)	Eastern Swiss Alps	46°32'N	09°49'E	2775-2840	0.74
	Oigrube	Western Austrian Alps	46°54'N	10°45E	2580-2810	1.5
	Reichenkar	Western Austrian Alps	47°03'N	11°02'E	2310-2750	3.15
	Weissenkar	Central Austian Alps	46°57'N	12°45E	2610-2720	0.08
	Hinteres Langtalkar (upper)	Central Austian Alps	46°59'N	12°46E	>2655	0.18
	Hinteres Langtalkar (lower)	Central Austian Alps	46°59'N	12°46E	<2655	2.22
	Düsen	Central Austian Alps	46°59'N	13° 17E	2540-2650	0.26
Delaloye, Lambiel, & Gärtner-Roer, 2010	Petit-Vélan	Valais Alps	46°05'N	07°50'E	2510-2820	3.0 - 10
	Aget	Valais Alps	46°05'N	07°50'E	2810-2890	0.1 - 0.3
	Mille	Valais Alps	46°05'N	07°50'E	2350-2440	< 0.1
	Lac des Vaux B	Valais Alps	46°05'N	07°50'E	2710-2780	0.3 - 1.0
	Lapires	Valais Alps	46°05'N	07°50'E	2640-2610	0.3 - 1.0
	Mont-Gelé B	Valais Alps	46°05'N	07°50'E	2600-2740	0.3 - 1.0
	Mont-Gelé C	Valais Alps	46°05'N	07°50'E	2620-2820	0.1 - 0.3
	Luels Rares	Valais Alps	46°05'N	07°50'E	2340-2420	0.1 - 0.3
	Tsarmine	Valais Alps	46°05'N	07°50'E	2460-2640	1.0 - 3.0
	Les Clessies	Valais Alps	46°05'N	07°50'E	2460-2600	0.1 - 0.3
	Becs-de-Bosson	Valais Alps	46°05'N	07°50'E	2610-2850	0.3 - 1.0
	Tsaté	Valais Alps	46°05'N	07°50'E	2680-2860	3.0 - 10
	Bonnard	Valais Alps	46°05'N	07°50'E	2840-3000	0.3 - 1.0
	HuHH1	Valais Alps	46°05'N	07°50'E	2630-2780	0.3 - 1.0
	HuHH3	Valais Alps	46°05'N	07°50'E	2515-2650	1.0 - 3.0
	Grosse Grabe	Valais Alps	46°05'N	07°50'E	2400-2700	3.0 - 10
	Gugla	Valais Alps	46°05'N	07°50'E	2600-2800	3.0 - 10
	Dirru	Valais Alps	46°05'N	07°50'E	2520-2650	3.0 - 10
	Chessi	Valais Alps	46°05'N	07°50'E	2500-2000	1.0 - 3.0
	Gänder	Valais Alps	46°05'N	07°50'E	2410-2770	3.0 - 10
	Jegi	Valais Alps	46°05'N	07°50'E	2460-2730	3.0 - 10
	Furggentälli	Bernese Alps	46°25'N	07°45E	2450-2650	0.3 - 1.0
	Grosses Gufer	Bernese Alps	46°25'N	07°45E	2260-2600	0.3 - 1.0
	Klein Furkahorn	Gotthard Region	46°33'N	08°34E	2630-2740	0.1 - 0.3
	Blaubergsee	Gotthard Region	46°33'N	08°34'E	2640-2700	0.1 - 0.3
	Gütsch	Gotthard Region	46°33'N	08°34'E	2190-2240	< 0.1
	Monte Prosa A	Gotthard Region	46°33'N	08°34'E	2430-2600	0.3 - 1.0
	Monte Prosa B	Gotthard Region	46°33'N	08°34'E	2450-2520	0.1 - 0.3
	Pizzo Nero	Tessin	46° 19'N	08°49'E	2660-2700	0.1 - 0.3
	Cavagnoli	Tessin	46° 19'N	08°49'E	2560-2800	0.3 - 1.0
	Ganoni di Schenadli	Tessin	46° 19'N	08°49'E	2470-2640	0.1 - 0.3
	Piancabella	Tessin	46° 19'N	08°49'E	2460-2560	0.1 - 0.3
	Stabbio di Largario	Tessin	46° 19'N	08°49'E	2300-2560	0.3 - 1.0
	Murtel	Grisons	46°45'N	09°30'E	2630-2800	< 0.1
	Marmugnun	Grisons	46°45'N	09°30'E	2660-2700	0.1 - 0.3
	Gupf	Grisons	46°45'N	09°30'E	2650-2700	0.3 - 1.0
	Chastelets	Grisons	46°45'N	09°30'E	2660-2700	0.3 - 1.0
	Muragl	Grisons	46°45'N	09°30'E	2460-2750	0.3 - 1.0
White, 1971	Arapaho	Colorado Front range	40°01'15"N	105°38'20"W	3570-3710	0.17
	Arapaho	Colorado Front range	40°01'15"N	105°38'20"W	3570-3710	0.06
	Arapaho	Colorado Front range	40°01'15"N	105°38'20"W	3570-3710	0.225
	Arapaho	Colorado Front range	40°01'15"N	105°38'20"W	3570-3710	0.02
	Arapaho	Colorado Front range	40°01'15"N	105°38'20"W	3570-3710	0.177
	Arapaho	Colorado Front range	40°01'15"N	105°38'20"W	3570-3710	0.062
	Arapaho	Colorado Front range	40°01'15"N	105°38'20"W	3570-3710	0.087
	Arapaho	Colorado Front range	40°01'15"N	105°38'20"W	3570-3710	0.055
	Arapaho	Colorado Front range	40°01'15"N	105°38'20"W	3570-3710	0.137
	Arapaho	Colorado Front range	40°01'15"N	105°38'20"W	3570-3710	0.005
	Arapaho	Colorado Front range	40°01'15"N	105°38'20"W	3570-3710	0.02
	Arapaho	Colorado Front range	40°01'15"N	105°38'20"W	3570-3710	0.062
	Arapaho	Colorado Front range	40°01'15"N	105°38'20"W	3570-3710	0.094
	Taylor	Colorado Front range	40° 16'30"N	105°40'15"W	3330-3540	0.035
	Taylor	Colorado Front range	40° 16'30"N	105°40'15"W	3330-3540	0.05
	Taylor	Colorado Front range	40° 16'30"N	105°40'15"W	3330-3540	0.045
	Taylor	Colorado Front range	40° 16'30"N	105°40'15"W	3330-3540	0.077
	Taylor	Colorado Front range	40° 16'30"N	105°40'15"W	3330-3540	0.072
	Taylor	Colorado Front range	40° 16'30"N	105°40'15"W	3330-3540	0.075
	Taylor	Colorado Front range	40° 16'30"N	105°40'15"W	3330-3540	0.04
	Taylor	Colorado Front range	40° 16'30"N	105°40'15"W	3330-3540	0.097
	Taylor	Colorado Front range	40° 16'30"N	105°40'15"W	3330-3540	0.08
	Taylor	Colorado Front range	40° 16'30"N	105°40'15"W	3330-3540	0.05
	Taylor	Colorado Front range	40° 16'30"N	105°40'15"W	3330-3540	0.035
	Taylor	Colorado Front range	40° 16'30"N	105°40'15"W	3330-3540	0.065
	Taylor	Colorado Front range	40° 16'30"N	105°40'15"W	3330-3540	0.025
	Taylor	Colorado Front range	40° 16'30"N	105°40'15"W	3330-3540	0.1
	Taylor	Colorado Front range	40° 16'30"N	105°40'15"W	3330-3540	0.065
	Taylor	Colorado Front range	40° 16'30"N	105°40'15"W	3330-3540	0.13
	Taylor	Colorado Front range	40° 16'30"N	105°40'15"W	3330-3540	0.155
	Taylor	Colorado Front range	40° 16'30"N	105°40'15"W	3330-3540	0.077
	Fair	Colorado Front range	40°03'50"N	105°39'20"W	3520-<3320	0.04
	Fair	Colorado Front range	40°03'50"N	105°39'20"W	3520-<3320	0.116
	Fair	Colorado Front range	40°03'50"N	105°39'20"W	3520-<3320	0.112
	Fair	Colorado Front range	40°03'50"N	105°39'20"W	3520-<3320	0.1
	Fair	Colorado Front range	40°03'50"N	105°39'20"W	3520-<3320	0.078
	Fair	Colorado Front range	40°03'50"N	105°39'20"W	3520-<3320	0.15
	Fair	Colorado Front range	40°03'50"N	105°39'20"W	3520-<3320	0.134
	Fair	Colorado Front range	40°03'50"N	105°39'20"W	3520-<3320	0.146
	Fair	Colorado Front range	40°03'50"N	105°39'20"W	3520-<3320	0.104
	Fair	Colorado Front range	40°03'50"N	105°39'20"W	3520-<3320	0.088
	Fair	Colorado Front range	40°03'50"N	105°39'20"W	3520-<3320	0.058
	Fair	Colorado Front range	40°03'50"N	105°39'20"W	3520-<3320	0.044
	Fair	Colorado Front range	40°03'50"N	105°39'20"W	3520-<3320	0.058
	Fair	Colorado Front range	40°03'50"N	105°39'20"W	3520-<3320	0.132
	Fair	Colorado Front range	40°03'50"N	105°39'20"W	3520-<3320	0.097

REFERENCES

Barsch, D. (1987). The problem of the ice-cored rock glacier. Rock glaciers. 45-53.

Barsch, D., (1996). Rock glaciers. Indicators for the present and former geoecology in high mountain environments. Springer, Berlin. Springer Series in Physical Environment. https://doi.org/10.1007/978-3-642-800093-1_3

Berthling, I., (2011) Beyond confusion: Rock glaciers as cryoconditioned landforms. Geomorphology. 131(3-4). https://doi.org/10.1016/j.geomorph.2011.05.002

Capps, S (1910). Rock Glaciers in Alaska. The Journal of Geology, 18(4), 359-375. https://doi.org/191.97.26.159

Clark, D. H., Steig, E. J., Potter, Jr., N. and Gillespie, A. R. (1998), Genetic variability of rock glaciers. Geografiska Annaler: Series A, Physical Geography, 80: 175-182. doi:10.1111/j.0435-3676.1998.00035.x

Delaloye, R. (2009). Recent interannual variations of rock glacier creep in the European Alps. *9th International Conference of Permafrost, Fairbanks, Alaska, 29. June 2008 - 03 July 2008*, 343-348.

Glen, J.W., (1955) The creep of polycrystalline ice. *Proceedings of the Royal Society of London. Series A. Mathematical and Physical Sciences*, *228*(1175), 519. https://doi.org/10.1098/rspa.1955.0066

Hopkins, N., Evenson, E., and Berti C., (2014). Low rates of horizontal deformation and thermokarst subsidence from D-InSAR Analysis of the Altar rock glacier, San Juan Province, Argentina

Haeberli, W. (1985). Creep of Mountain Permafrost: Internal Structure and Flow of Alpine Rock Glaciers. Mitteilungen der Versuchan-stalt fur Wasserbau, Hydrologie und Glaziologie (Zürich). 77.

Hinojosa L.F., and Villagran C. (1997). Historia de los bosques del sur de Sudamerica, I: antecedents paleobotanicos, geologicos y climaticos del Terciario del cono sur de America. Rev. Chil. Hist. Nat. 70,225–39

Houston J., and Hartley A.J. (2003). The central Andean West-Slope rainshadow and its potential contribution to the origin of Hyper-Aridity in the Atacama Desert. Int. J. Climatol. 23,1453–64

Kane, R. (2014) Using terrestrial laser scanning for differential measurement of interannual rock glacier movement in the Argentine dry Andes. Unpubl. Masters Thesis, University of Delaware.

Oncken, O., Chong G., Franz G., Giese P., Götze H., Ramos V., Strecker M., and Wigger P. (2006) The Andes: Active Subduction Orogeny. Springer. https://dio.org/10.1007/2F978.3

Schreiber, E. (2015) Modeling the distribution of mountain permafrost in the Central Andes, San Juan, Argentina. Unpubl. Masters Thesis, University of Delaware.

Trzinski, A. (2017). Physiographic and climatic controls on the spatial distribution of rock glaciers and periglacial landforms in the Dry Andes, San Juan, Argentina. Unpubl. Masters Thesis, University of Delaware.

Wahrhaftig, C., and Cox, A. (1959) Rock glaciers in the Alaska Range. Bulletin of the Geological Society of America 70(4): 383-436

Yosikawa, K., and Hinzman, L. (2003) Shrinking Thermokarst Ponds and Groundwater Dynamics in Discontinuous Permafrost near Council, Alaska. Permafrost Periglac. Process. 14: 151–160

Appendix A

MOTION

The following pages display the motion of the El Altar, QDM and Los Azules rock glaciers. Motion is depicted with easting displayed on the x-axis and northing displayed on the y-axis. Each year is labeled with a unique marker and line symbol. The El Altar rock glacier labels begin with MO, the QDM rock glacier labels begin with QMRG, and the Los Azules motion figure

labels begin with MAW. Note the varying scales depicted to make use of available space. The majority of the El Altar markers contain a 50 cm × 50 cm scale except for MO18 and MO19, which are both scaled to 1 m × 1 m. QMRG-5L contain a scale of 1 m × 1 m for QMRG-5L, 1.5 m × 1.5 m for QMRG-6L, and 50 cm × 50 cm for QMRG-7L. For Los Azules, MAE3, MAW3 and MAW5 were displayed at a 20 cm × 20 cm scale, whereas MAW1 and MAW2 were displayed at a 50 cm × 50 cm scale. Stake movement was measured for varying amounts of time based on assessment of need.

Because the Andes are an tectonically active zone, stable rocky surfaces next to the rock glaciers serves as stable locales for determining relative movements both within and between annual surveys. The following paragraph discusses the 4 remaining stakes used as stable locales which are located in close proximity to the rock glacier, but not directly on it. There is no slope calculation for these stakes because they were not included in the flight path. MO15 is the westernmost of all movement stakes. The fastest recorded movement was 0.001 m/month, and the slowest recorded movement was negligible (0.000 m/month). Following that, MO14, which is located southeast of MO15, moves at a yearly average of 0.012 m. The fastest recorded movement was 0.003 m/month, and the slowest recorded movement was 0.001 m/month. The southernmost monitoring stake (MO13) moves at an average rate of 0.003 m/year. The fastest recorded movement was 0.001 m/month, and the slowest

recorded movement was negligible (0.000 m/month). The remaining monitoring stake (MO12), which is located at the base of the eastern portion of the rock glacier, moves at an average yearly rate of 0.006 m/year. The fastest recorded movement was 0.002 m/month, and the slowest recorded movement was also negligible (0.000 m/month).

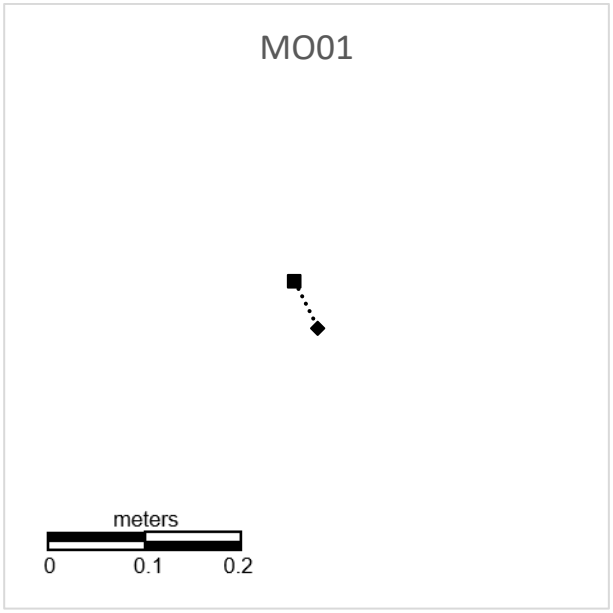
MO01
meters
0
0.1
0.2

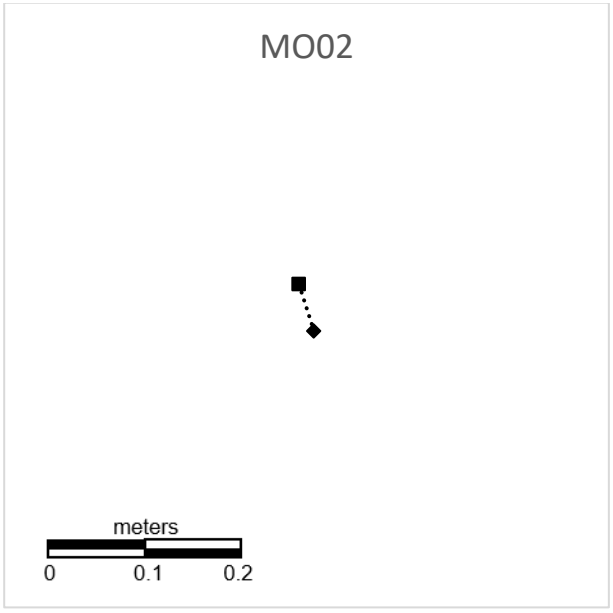
MO02
meters
0
0.1
0.2

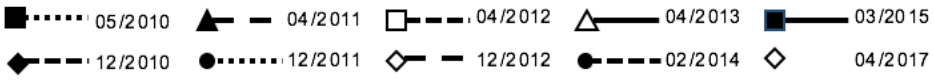
05/2010
04/2011
04/2012
04/2013
03/2015
12/2010
12/2011
12/2012
02/2014
04/2017

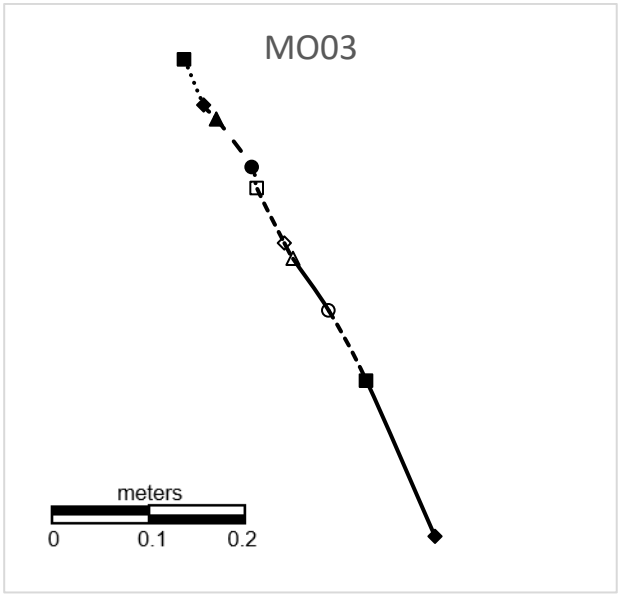
MO03
meters
0
0.1
0.2

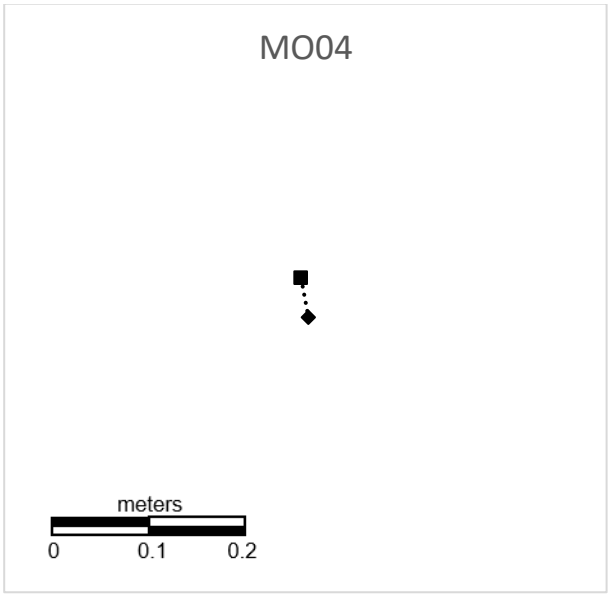
MO04
meters
0
0.1
0.2

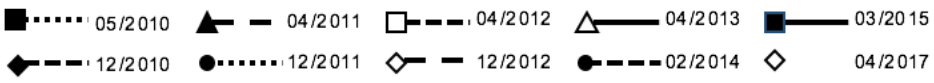
05/2010
04/2011
04/2012
04/2013
03/2015
12/2010
12/2011
12/2012
02/2014
04/2017

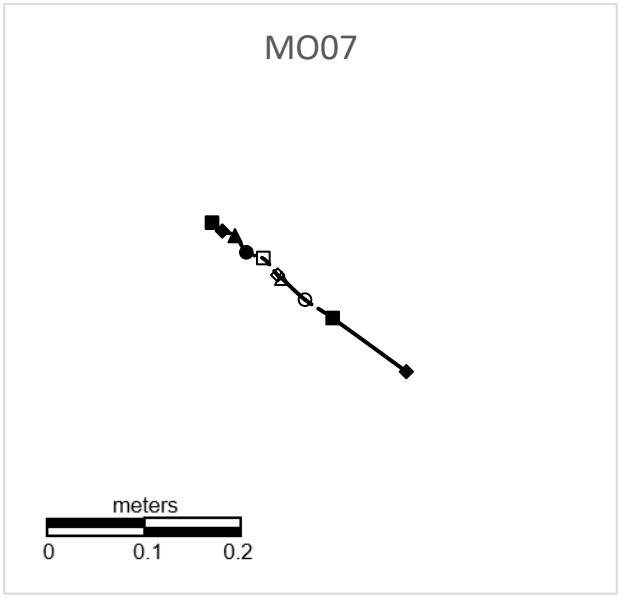
MO07
meters
0
0.1
0.2

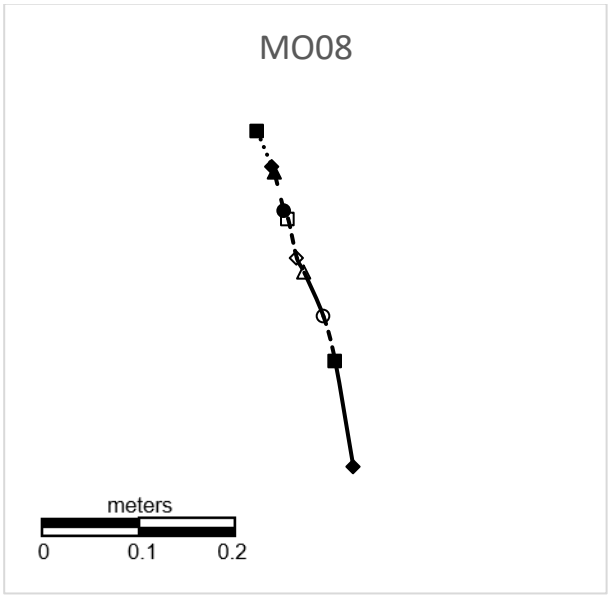
MO08
meters
0
0.1
0.2

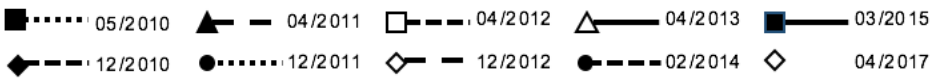
05/2010
04/2011
04/2012
04/2013
03/2015
12/2010
12/2011
12/2012
02/2014
04/2017

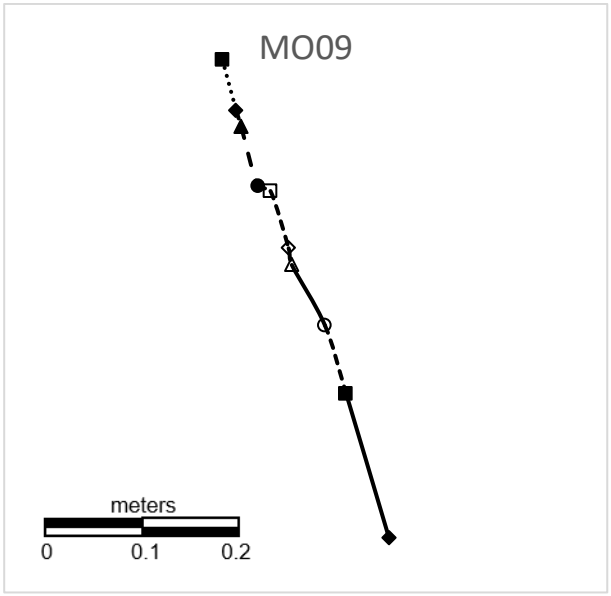
MO09
meters
0
0.1
0.2

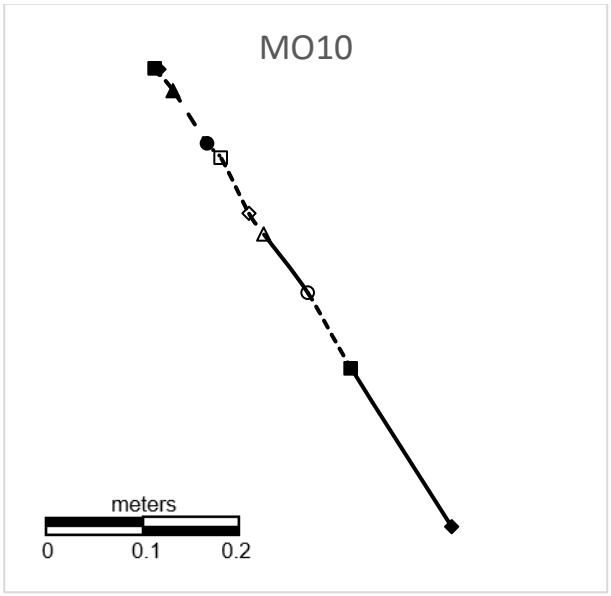
MO10
meters
0
0.1
0.2

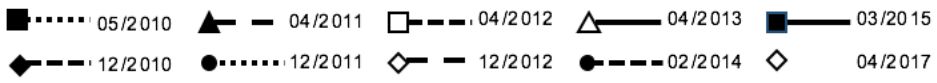
05/2010
04/2011
04/2012
04/2013
03/2015
12/2010
12/2011
12/2012
02/2014
04/2017

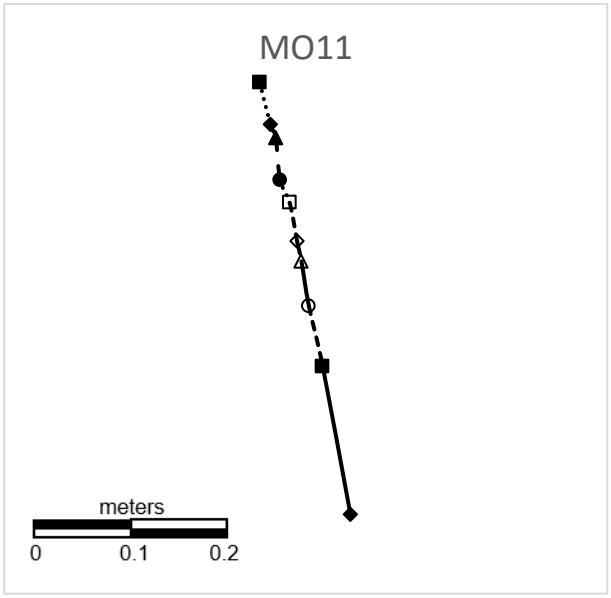
MO11
meters
0
0.1
0.2

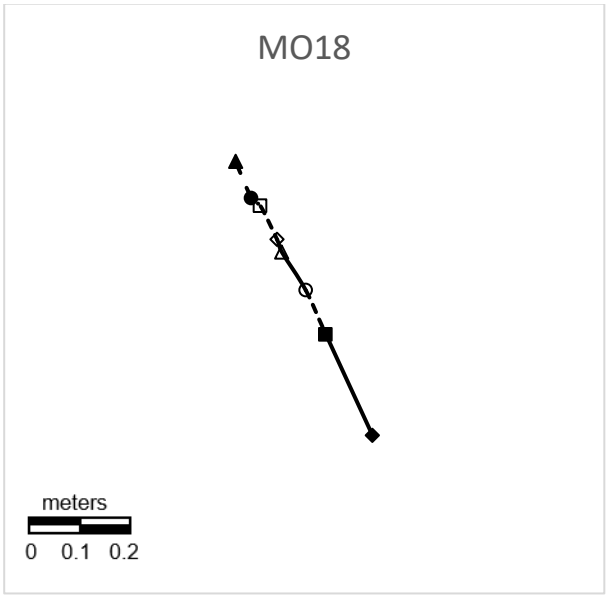
MO18
meters
0
0.1
0.2

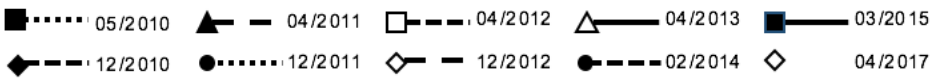
05/2010
04/2011
04/2012
04/2013
03/2015
12/2010
12/2011
12/2012
02/2014
04/2017

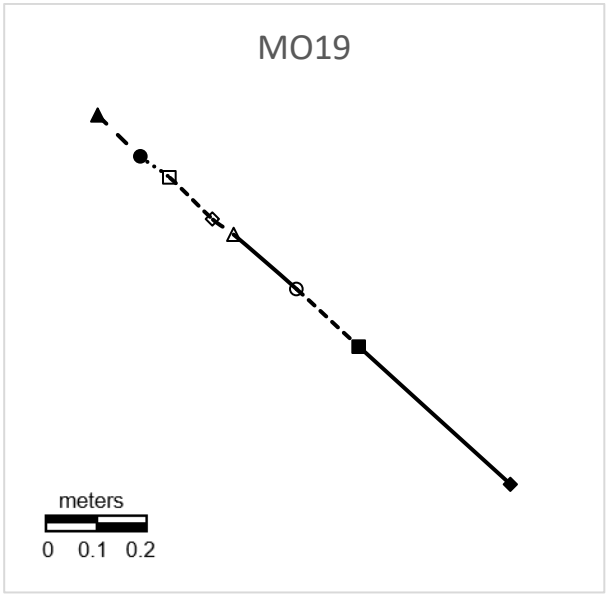
MO19
meters
0 0.1 0.2

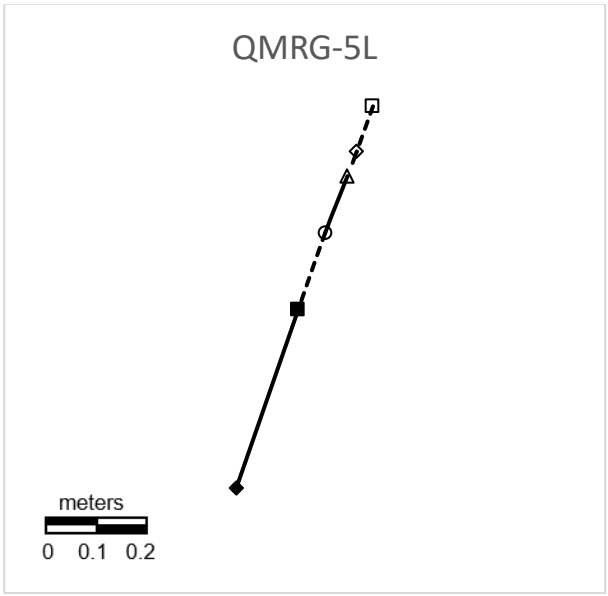
QMRG-5L
meters
0 0.1 0.2

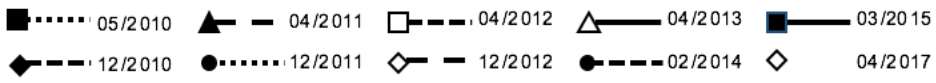
05/2010
04/2011
04/2012
04/2013
03/2015
12/2010
12/2011
12/2012
02/2014
04/2017

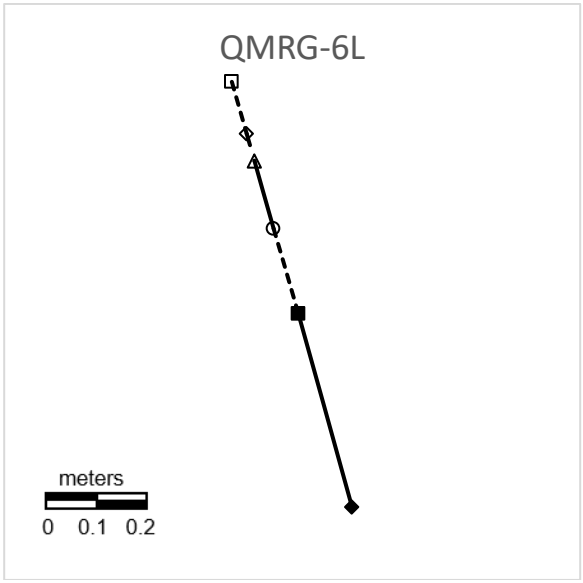
QMRG-6L
meters
0 0.1 0.2

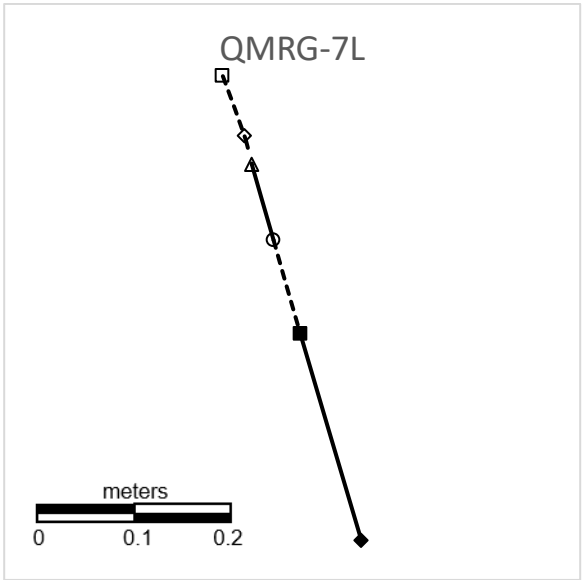
QMRG-7L
meters
0 0.1 0.2

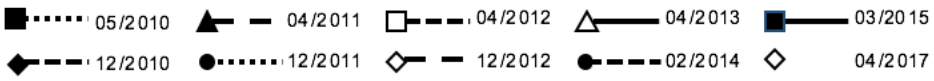
05/2010
04/2011
04/2012
04/2013
03/2015
12/2010
12/2011
12/2012
02/2014
04/2017

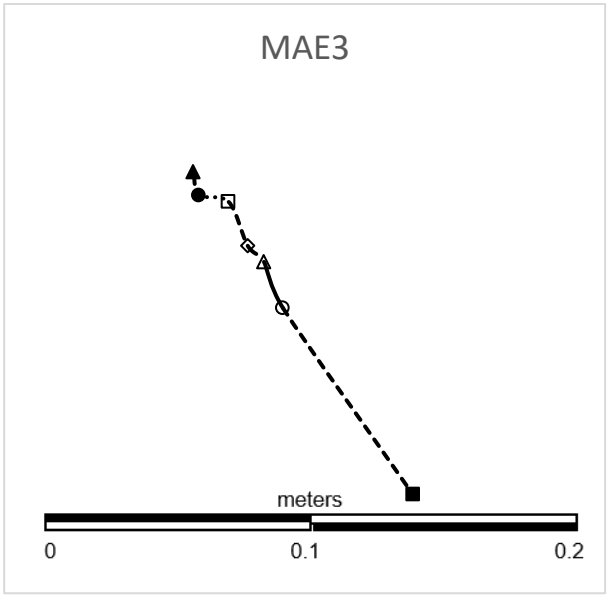

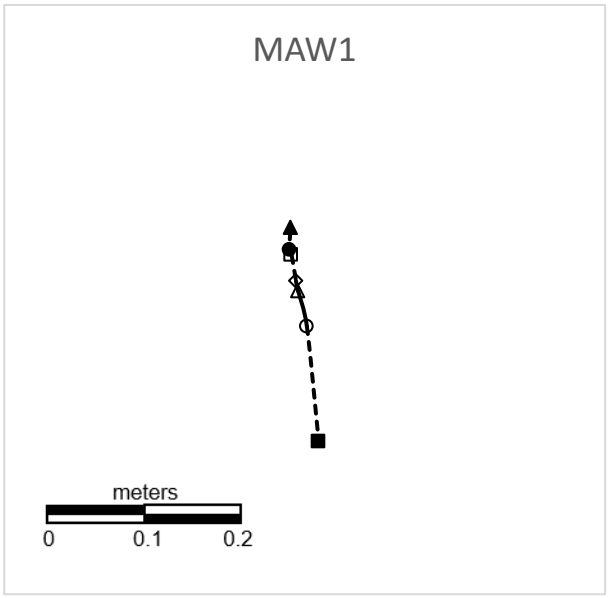

05/2011 04/2012 03/2013 03/2017
01/2012 12/2012 02/2014

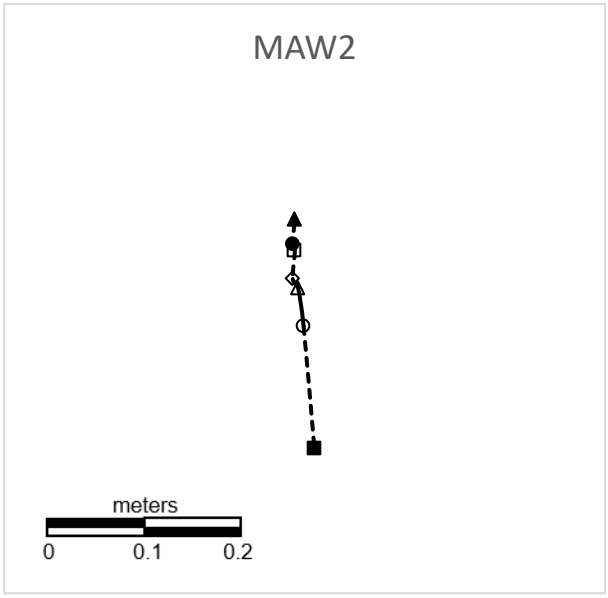
MAW2
meters
0
0.1
0.2

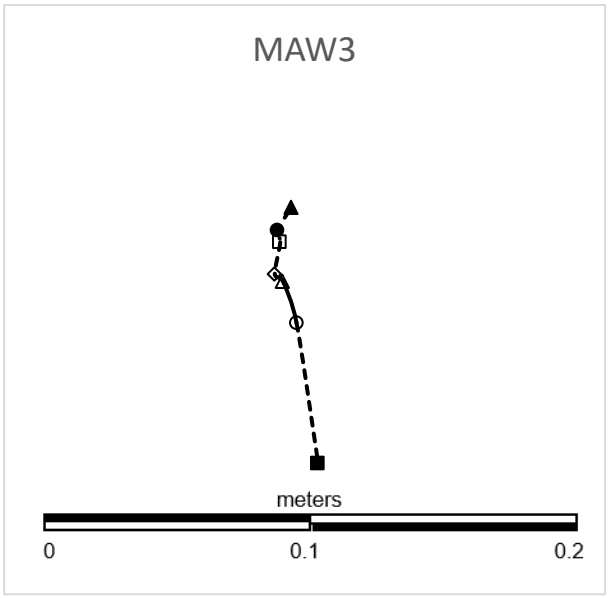
MAW3
meters
0
0.1
0.2

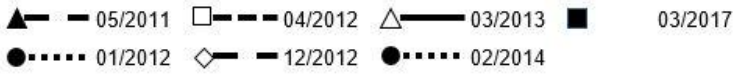
05/2011
04/2012
03/2013
03/2017
01/2012
12/2012
02/2014

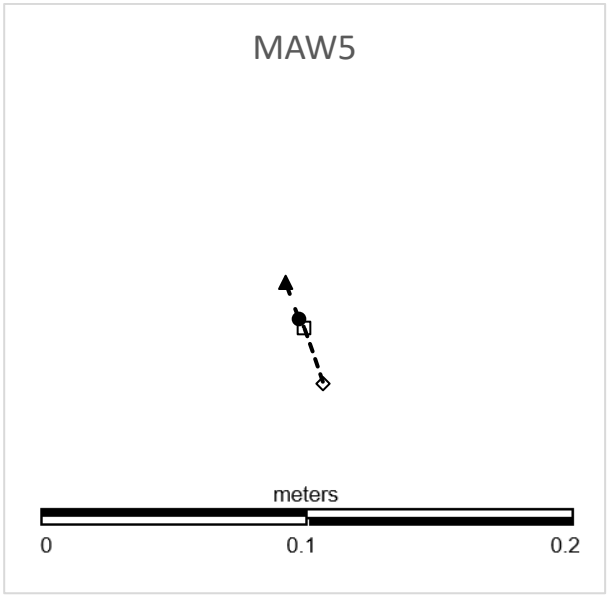
MAW5
meters
0
0.1
0.2

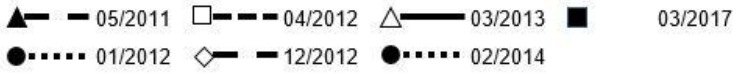
05/2011
04/2012
03/2013
03/2017
01/2012
12/2012
02/2014